

Confusion limited surveys: using WISE to quantify the rarity of warm dust around *Kepler* stars

G. M. Kennedy* & M. C. Wyatt

Institute of Astronomy, University of Cambridge, Madingley Road, Cambridge CB3 0HA, UK

12 November 2018

ABSTRACT

We describe a search for infra-red excess emission from dusty circumstellar material around 180,000 stars observed by the *Kepler* and WISE missions. This study is motivated by i) the potential to find bright warm disks around planet host stars, ii) a need to characterise the distribution of rare warm disks, and iii) the possible identification of candidates for discovering transiting dust concentrations. We find about 8,000 stars that have excess emission, mostly at $12\mu\text{m}$. The positions of these stars correlate with the $100\mu\text{m}$ background level so most of the flux measurements associated with these excesses are spurious. We identify 271 stars with plausible excesses by making a 5MJy/sr cut in the IRAS $100\mu\text{m}$ emission. The number counts of these excesses, at both 12 and $22\mu\text{m}$, have the same distribution as extra-Galactic number counts. Thus, although some excesses may be circumstellar, most can be explained as chance alignments with background galaxies. The one exception is a $22\mu\text{m}$ excess associated with a relatively nearby A-type star that we were able to confirm because the disk occurrence rate is independent of stellar distance. This detection implies a disk occurrence rate consistent with that found for nearby A-stars. Despite our low detection rate, these results place valuable upper limits on the distribution of large mid-infrared excesses; e.g. fewer than 1:1000 stars have $12\mu\text{m}$ excesses (F_{obs}/F_{\star}) larger than a factor of five. In contrast to previous studies, we find no evidence for disks around 1790 stars with candidate planets (we attribute one significant $12\mu\text{m}$ excess to a background galaxy), and no evidence that the disk distribution around planet hosts is different to the bulk population. Higher resolution imaging of stars with excesses is the best way to rule out galaxy confusion and identify more reliable disk candidates among *Kepler* stars. A similar survey to ours that focusses on nearby stars would be well suited to finding the distribution of rare warm disks.

Key words: planets and satellites: formation — stars:individual, HD 69830, BD +20 307, HD 172555, η Corvi, HIP 13642, KIC 7345479

1 INTRODUCTION

Kepler (Borucki et al. 2003) is revolutionising our perspective on extra-Solar planets (e.g. Holman et al. 2010; Lissauer et al. 2011a; Batalha et al. 2011; Doyle et al. 2011; Howell et al. 2011; Borucki et al. 2012) and will likely yield many Earth-sized planets in the terrestrial zones of their host stars. Like the Solar System, these planetary systems will comprise not only planets, but also smaller objects that for one reason or another did not grow larger. In the Solar System these make up the Asteroid and Kuiper belts, along with other populations such as the Oort cloud, and Trojan and irregular satellites. Characterisation of these populations has been critical to building our understanding of how the Solar System formed. For example, one of the primary validation methods of the so-called “Nice” model for the origin of the outer Solar System’s

architecture has been the reproduction of these minor body populations and their properties (e.g. Morbidelli et al. 2005; Levison et al. 2008; Nesvorný et al. 2007).

The exquisite detail with which the Solar System minor body populations are characterised is made clear when they are contrasted with their extra-Solar analogues, collectively known as “debris disks.” First discovered around Vega (Aumann et al. 1984), they are almost always detected by unresolved infra-red (IR) emission, visible as an excess above the stellar photosphere. Detection of an excess at multiple wavelengths yields the dust temperature, and thus the approximate radial distance from the star (to within a factor of a few). The radial location can be refined further when spectral features are present (e.g. Lisse et al. 2007). However, because the temperature of a dust or ice grain depends on size, the true radial location (and any radial, azimuthal, or vertical structure) can generally only be found by resolved imaging (e.g. Smith & Terrielle

* Email: gkennedy@ast.cam.ac.uk

1984; Kalas et al. 2005) or interferometry (e.g. Absil et al. 2006; Smith et al. 2009).

It is therefore difficult to draw links between the regions of planetary systems occupied by planets and small bodies, and if and how they interact. The best examples of extrasolar systems where known dust and planets are likely to interact are β Pictoris, Fomalhaut, and HR 8799 (Burrows et al. 1995; Mouillet et al. 1997; Kalas et al. 2005, 2008; Marois et al. 2008; Su et al. 2009; Moro-Martín et al. 2010). In these cases, the spatial dust distribution is fairly well known because the disk is resolved, but the orbits of the planets, which were only discovered recently with direct imaging, are not. These are rare cases however, and typically the search for links between the major and minor body components of extra-Solar planetary systems means asking whether the presence of one makes the presence of the other more or less likely. So far no statistically significant correlation between the presence of planets and debris has been found (Kóspál et al. 2009; Bryden et al. 2009; Dodson-Robinson et al. 2011). However, there is new tentative evidence that nearby stars with low-mass planetary systems are more likely to harbour debris than those with no planet detections (Wyatt et al, in press), an exciting possibility that has only been achievable recently with better sensitivity to such planetary systems around nearby stars.

One of the key limiting factors in the search for links between debris and planets is the small number of stars known to host both. Two recent *Spitzer* surveys observed about 150 planet host stars, of which about 10% were found to have disks (Bryden et al. 2009; Dodson-Robinson et al. 2011). The small number of disk detections is therefore the product of the number of nearby stars known to host planets that could be observed with *Spitzer*, and the $\sim 10\%$ disk detection rate (for both planet and non-planet host stars). One way to sidestep this problem is therefore to look for disks around a much larger sample of planet host stars; the *Kepler* planet host candidates (Borucki et al. 2011; Batalha et al. 2012).

The method we use to look for disks in this study is to find infra-red (IR) excess emission above that expected from the stellar photosphere. An IR excess is usually interpreted as being thermal emission from an Asteroid or Kuiper-belt analogue, which is heated by the star it orbits. We use photometry from the Wide-field Infrared Survey Explorer (WISE) mission’s (Wright et al. 2010) all-sky catalogue, which is most sensitive to dust in the terrestrial region of Sun-like stars. Three properties of warm dust at these relatively close radial distances provide motivation.

First, this warm dust, if discovered, is located in the vicinity of the planets being discovered with *Kepler*. Currently, only one system, HD 69830, is known to host both a planetary system in the terrestrial region and warm dust (Beichman et al. 2005; Lovis et al. 2006). The origin of this dust is unclear, but given the proximity to the planetary system is plausibly related (Lisse et al. 2007; Beichman et al. 2011). Through discovery of similar systems the links between planets and warm dust can be better understood.

For planets discovered by *Kepler*, the knowledge that a transiting planetary system is almost exactly edge-on provides the second motivational aspect. If planets pass in front of the host star, so will coplanar minor body populations. Indeed, the discovery of systems where multiple planets transit their stars (e.g. Holman et al. 2010; Lissauer et al. 2011a,b) provides striking evidence that the Solar System’s near-coplanar configuration is probably typical. While transits of individual small bodies will be impossible to detect, it may be possible to detect concentrated populations that arise from a recent collision (Kenyon & Bromley 2005) or perturbations by planets (Stark 2011). The dust must reside on a fairly close orbit—

within a few AU—to allow multiple transits within the mission lifetime. Thus, the WISE sensitivity to terrestrial dust, and likely difficulties in discerning dust transits from other instrumental and real effects, mean that the odds of finding dust transits might be maximised by the prior identification of dusty systems.

Finally, but most importantly, detections of terrestrial dust are rare (e.g. Aumann & Probst 1991; Hines et al. 2006; Bryden et al. 2006; Beichman et al. 2006b). Because only a few such systems are known, their occurrence rate is poorly constrained. More discoveries are therefore needed to add to our understanding of the processes that create it. The collision rate in a debris disk is proportional to the orbital period, so warm terrestrial debris disks decay to undetectable levels rapidly, hence their rarity. Indeed, the few that are known are usually thought to be the result of recent collisions, and thus transient phenomena (e.g. HD 69830, HD 172555, BD +20 307, η Corvi, HD 165014, HD 169666, HD 15407A Beichman et al. 2005; Song et al. 2005; Wyatt et al. 2007; Lisse et al. 2009; Moór et al. 2009; Fujiwara et al. 2010; Lisse et al. 2011; Fujiwara et al. 2012). Possible scenarios include objects thrown into the inner regions of a planetary system from an outer reservoir (Gaidos 1999; Wyatt et al. 2007; Booth et al. 2009; Raymond et al. 2011; Bonsor & Wyatt 2012), or the remnant dust from a single catastrophic collision (Song et al. 2005; Beichman et al. 2005; Weinberger et al. 2011).

Clearly, there are reasons that discovery of debris in the terrestrial regions of known planetary systems is important. However, because WISE is sensitive to the rarest and brightest disks around *Kepler* stars, the third point above is of key importance. As stars become more distant, they and their debris disks become fainter, and the number of background galaxies at these fainter flux levels increases. Thus, the bulk of the stars in the *Kepler* field, which lie at distances of hundreds to thousands of parsecs may not be well suited to debris disk discovery. Practically, the importance of contamination depends on the galaxy contamination frequency relative to the disk frequency (i.e. only if disks are too rare will they be overwhelmed by contamination). *Therefore, because the occurrence rate of the rare disks that WISE is sensitive to is unknown, whether Kepler stars are a good sample for disk detection with WISE is also unknown.*

Characterising the occurrence rate of rare bright disks is therefore the main goal of this study, because this very distribution sets what can be discovered. While the sample of *Kepler* stars is not specifically needed for this goal, there is the possibility that the disk occurrence rate is higher for stars that host low-mass planets. Such a trend could make this particular sub-sample robust to confusion, even if the general population is not.

An additional potential issue specific to the *Kepler* field is the importance of the Galactic background. High background regions are sometimes avoided by debris disk observations because they make flux measurement difficult, and can even mask the presence of otherwise detectable emission. Unfortunately this issue cannot be avoided for the present study, as the *Kepler* field is necessarily located near the Galactic plane to maximise the stellar density on the sky.

In what follows, we describe our search for warm excesses around $\sim 180,000$ stars observed by *Kepler* using the WISE catalogue. We first outline the data used in this study in §2 and in §3 describe our SED fitting method for finding excesses and the various issues encountered. We discuss the interpretation of these excesses in §4, and place our findings in the context of disks around nearby stars in §5. We discuss the disk-planet relation, rarity of warm bright excesses, and some future prospects in §6 and con-

clude in §7. Readers only interested in the outcome of this search may wish to skip the details described in §§2-3.

2 CATALOGUES

The *Kepler* mission is observing $\sim 200,000$ stars near the Galactic plane to look for planets by the transit method (Borucki et al. 2003). The *Kepler* field of view (FOV) covers about 100 square degrees and is rotated by 90° every three months. Not all stars are observed in all quarters, but Figure 1 shows that the focal plane has four-fold rotational symmetry (aside from the central part), so most will be visible for the mission lifetime. Stars observed by *Kepler* are brighter than about 16th magnitude and selected to maximise the chance of transit detection and follow up (Batalha et al. 2010). The stars are drawn from the Kepler Input Catalogue (KIC), which contains optical photometry, cross-matched 2MASS IDs, and stellar parameters for millions of objects within the FOV (Brown et al. 2011).

The entire *Kepler* FOV is covered by the all-sky WISE mission (Wright et al. 2010), as shown by the coloured dots in the right panel of Figure 1. The scanning strategy used by WISE means that the sky coverage varies, and is highly redundant at the ecliptic poles (see Jarrett et al. 2011). WISE photometry comprises four bands with isophotal wavelengths of 3.4, 4.6, 12, and $22\mu\text{m}$ (called W1-4). The sensitivity is fairly well suited to stars observed by *Kepler*, with 5σ sensitivities of 17.1, 15.7, 11.4, and 8 magnitudes for 8 frames in W1-4 (corresponding to 44, 93, 800, and $5500\mu\text{Jy}$ respectively).

2.1 Cross matching

There were 189,998 unique KIC objects observed in quarters 1-6 of the mission, which we refer to as Kepler OBServed objects,¹ or “KOBs”. These KOBs are matched with three photometric catalogues: Tycho 2 (Høg et al. 2000), the 2MASS Point Source Catalogue (Skrutskie et al. 2006), and the WISE all-sky catalogue (Wright et al. 2010). Matching with 2MASS is straightforward because designations are already given in the KIC. The relevant 189,765 rows were retrieved using Vizier.² Tycho 2 objects were matched using a $1''$ search radius and retaining only the closest object, again using the Vizier service. This match returned 13,430 objects. The KIC itself contains photometry in SDSS-like bands ($ugriz$ each with 1092, 189383, 189829, 186908, 177293 KOB measurements respectively) and a DDO51-like narrowband filter centered on 510nm (with 176170 measurements). Finally, WISE objects are matched using the IPAC Gator service³ with a radius of $1''$, which returns 181,004 matches. It is these 181,004 objects that are the focus of this study.

3 FINDING EXCESSES

The method used to identify debris disk candidates is fitting stellar atmospheric model spectral energy distributions (SEDs) to the available photometry (known as “SED fitting”). Optical and near-IR bands are used to fit the stellar atmosphere and make predictions of the photospheric flux at longer wavelengths, which are

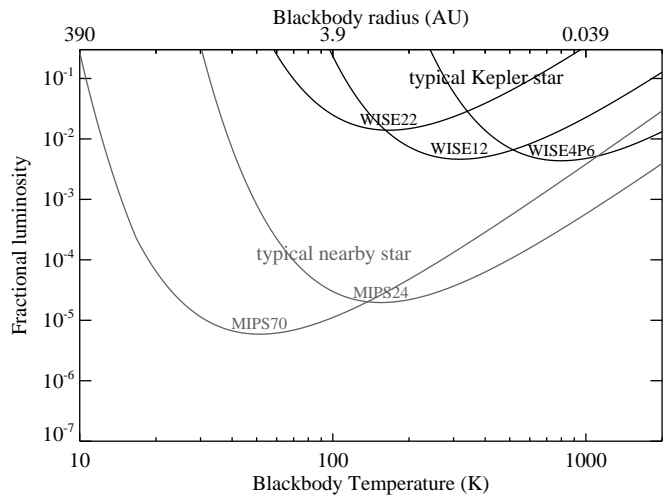


Figure 2. WISE W2-4 ($4.6\text{--}22\mu\text{m}$) 3σ sensitivity to blackbody emission around a typical star in the *Kepler* field, a 5460K star with $K_s = 13.5\text{mag}$ (black lines). Also shown is the sensitivity with MIPS at 24 and $70\mu\text{m}$ to 55 Cancri, a typical nearby star at 12pc with $K_s \approx 4.2$ (grey lines).

compared to the WISE observations. An IR excess indicates the possible presence of thermal emission from circumstellar dust, but can also arise for other reasons; overestimated flux due to a high Galactic background, chance alignment with a background galaxy that has a cooler spectrum than a star, and poor photospheric prediction are three examples. Excesses are usually quantified in two ways: the first is the flux ratio in a band B

$$R_B = F_B / F_{\star B}, \quad (1)$$

where F_B is the photometric measurement and $F_{\star B}$ is the photospheric prediction. The flux from the disk is therefore

$$F_{\text{disk}, B} = (R_B - 1) F_{\star B}. \quad (2)$$

The second is the excess significance,⁴

$$X_B = \frac{F_B - F_{\star B}}{\sqrt{\sigma_B^2 + \sigma_{\star B}^2}}, \quad (3)$$

where each σ is the photometric or stellar photospheric uncertainty. Typically a star is said to have excess emission when $X_B > 3$, though other (usually higher) values appropriate to the sample in question may be used.

Figure 2 illustrates the sensitivity of WISE to blackbody emission around a “typical” KOB; a 5460K star with $K_s = 13.5\text{mag}$. Only disks that have a combination of fractional luminosity ($f = L_{\text{disk}}/L_{\star}$) and temperature that lies above the line for a specific band can be detected in that band. Disks detected at a single wavelength lie somewhere along a single curve similar to (but above) those shown, and may be constrained by non-detections at other wavelengths (e.g. Figure 9 of Bryden et al. 2006). Temperatures can only be derived for disks that lie above multiple lines (i.e. are detected at multiple wavelengths). Compared to the MIPS observations of the nearby (12pc) star 55 Cancri (Trilling et al. 2008), the WISE sensitivity is much reduced. While MIPS $24\mu\text{m}$ observations are generally “calibration limited” by the precision of the

¹ Retrieved from <http://archive.stsci.edu/pub/kepler/catalogs/>

² <http://vizier.u-strasbg.fr/viz-bin/VizieR>

³ <http://irsa.ipac.caltech.edu/Missions/wise.html>

⁴ This quantity is usually called usually called χ_B , but we instead dub it X_B to avoid confusion with the goodness of fit indicator χ^2 . In this study we usually use the term “excess significance” instead of the symbol.

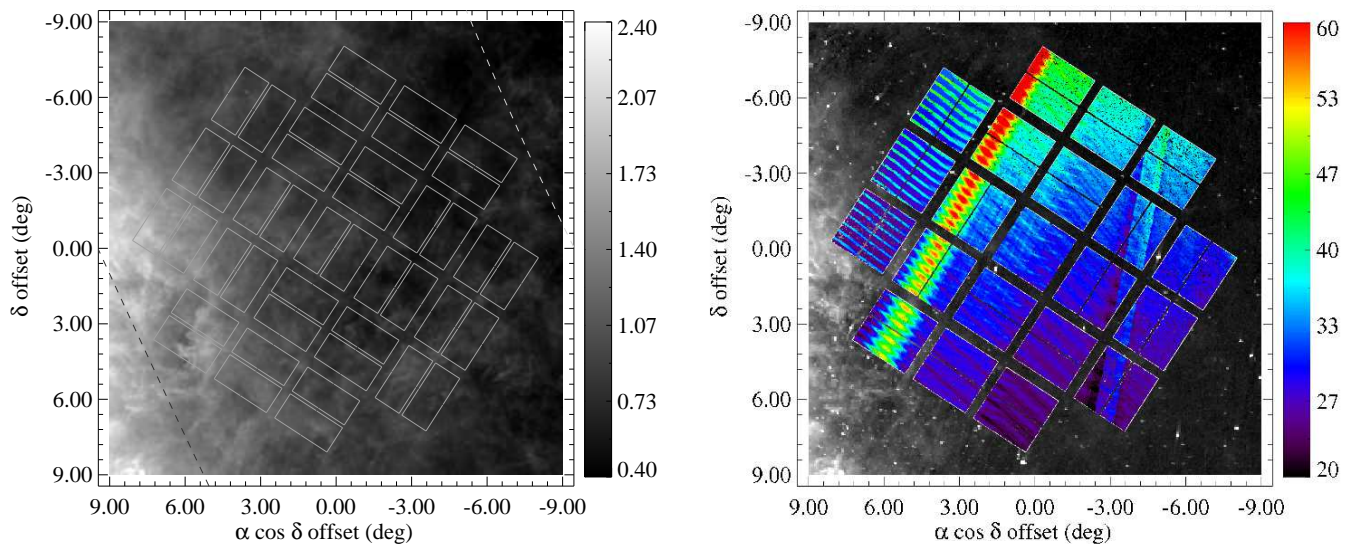


Figure 1. Kepler field of view (rectangles) with IRAS 100 μm (left panel, scale is log MJy/sr) and 25 μm (right panel) IRIS maps as background (Miville-Deschênes & Lagache 2005). North is up and East is left. The Galactic plane is towards the South-East, and in the left panel galactic latitudes of 5 and 22 $^\circ$ are shown as dashed lines. The WISE W1 mean pixel coverage in frames (called “w1cov” in the catalogue, coloured dots and scale) is shown in the right panel. Nearly all objects are observed by 20-60 frames, those with less or more have the colour at the respective end of the colour scale.

stellar photospheric predictions (i.e. $\sigma_{\star\text{B}} \gg \sigma_{\text{B}}$), WISE can at best detect a flux ratio of about 50 at 22 μm for the example shown here (so is “sensitivity limited” and $\sigma_{\star\text{B}} \ll \sigma_{\text{B}}$, see Wyatt 2008, for further discussion of sensitivity vs. calibration limited surveys). The WISE 22 μm observation is actually slightly deeper than the MIPS 24 μm one (both are sensitive to about 1mJy), so the reason for the difference in disk sensitivity is simply the brightness of the star. The radial scale shows that WISE is well suited to finding excesses with large fractional luminosity that lie within the terrestrial planet zone of Sun-like stars. To detect dust at larger distances would require either much greater sensitivity and/or longer wavelength data.

Because the sensitivity depends strongly on the brightness of the star, it also varies widely for KOBs. For the nearest and brightest stars the sensitivity is about two orders of magnitude better than shown for the KOB in Figure 2. However, the longest WISE wavelength is 22 μm , so even for the brightest stars the sensitivity to disks cooler than 100K drops significantly. Therefore, regardless of brightness, the wavelength range of WISE and the brightness of most KOBs means that any detections will be due to very luminous warm excesses. It is less likely that the Wein side of cooler emission will be detected because much higher fractional luminosities are required (i.e. the curves in Figure 2 rise very steeply to cooler temperatures and larger radii).

3.1 SED fitting

Our SED fitting method uses filter bandpasses to compute synthetic photometry and colour corrections for the stellar models, which are fit to observed photometry by a combination of brute force grids and least-squares minimisation. We use Phoenix AMES-Cond models from the Gaia grid (Brott & Hauschildt 2005), which cover a wide range of stellar parameters. However, these models only have $T_{\text{eff}} < 10,000\text{K}$, so stars pegged at this temperature are re-fit with Kurucz models (Castelli & Kurucz 2003). Previous efforts for the *Herschel* (Pilbratt et al. 2010) Disc Emission via a Bias-free

Reconnaissance in the Infrared/Submillimetre (DEBRIS) Key Programme (e.g. Matthews et al. 2010) have found that there is little or no difference between these models in terms of photospheric predictions for A-stars.

In addition to being near the Galactic plane, most stars observed by *Kepler* are hundreds to a few thousands of parsecs distant, so are reddened by interstellar dust. The 100 and 25 μm IRIS maps⁵ in Figure 1 show that cool emission from dust generally increases towards the Galactic plane, but also varies on scales much smaller than the *Kepler* FOV. We correct for this effect using the Rieke & Lebofsky (1985) reddening law.

There are five possible stellar parameters to include in the SED fitting: the effective temperature (T_{eff}), surface gravity ($\log g$), metallicity ([M/H]), reddening (A_V), and the solid angle of the star (Ω_{\star}). The stellar radius R_{\star} can subsequently be estimated from A_V by adopting some model for Galactic reddening (e.g. Brown et al. 2011) or by assuming the star has a specific luminosity class. In early SED fitting runs where all parameters were left free, models were commonly driven to implausible regions of parameter space in order to minimise the χ^2 . Similar issues lead Brown et al. (2011) to use a Bayesian approach, with priors based on observed stellar populations. Rather than duplicate and/or verify their method, we use some of their KIC stellar parameters as described below because our goal is to obtain the best photospheric prediction in WISE bands, not to derive stellar parameters.

Verner et al. (2011) show that the KIC gravities systematically differ from those derived by astroseismology by about 0.23dex, though unfortunately the discrepancy is strongest for those with $\log g > 4$ (i.e. dwarfs). In order to reduce the number of fitted parameters, we therefore fix $\log g$ in our fitting to the KIC value minus 0.23dex. Where no $\log g$ is tabulated, we set it to 4.5, appropriate for the Solar-type stars that make up the bulk of KOBs. To

⁵ Retrieved from <http://skyview.gsfc.nasa.gov/>.

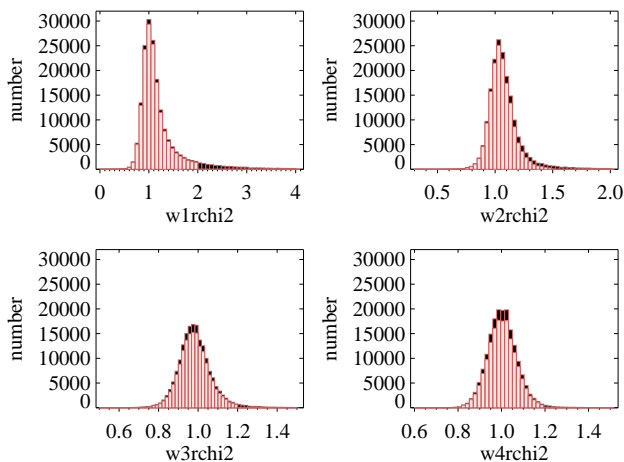


Figure 3. Goodness of fit quality for WISE source extraction in bands W1-4 ($w1, 2, 3, 4rchi2$). The non-Gaussian W1 distribution is an indication of confusion with nearby sources. The black histograms show all WISE sources, and the pink histograms show those remaining after the cut in goodness of fit described in the text.

further reduce the number of parameters, we also fix $[M/H]$ to the KIC value.

We use least squares minimisation to find an adequately fitting model, starting with the parameters tabulated in the KIC. When no parameters are given (most likely because a good fit could not be found for the KIC, [Brown et al. 2011](#)), we do a grid search over T_{eff} and Ω_* at $A_V = 0$ to find an initial fit, and then iterate to the best fit with these as free parameters (we apply a cut in fit quality below so if the fits remain poor the stars are excluded).

We use photometric bands up to and including WISE W1 to fit the stellar atmosphere. Including W1 in the stellar fit is reasonable because main-sequence stars rarely show excesses shortward of about $10\mu\text{m}$. In fact, bands such as IRAS $12\mu\text{m}$ and AKARI $9\mu\text{m}$ can usually be used to fit the photosphere, and it is only in rare cases, mostly for A-type stars, that these bands show an excess. In the present case however, the sample is two to three orders of magnitude larger than a typical debris disk survey, and our goal is to find rare excesses in these bands.

3.1.1 Discarding suspect and poor photometry

Care must be taken when using the photometry from the 2MASS and WISE catalogues. The very large number of sources means that small issues that are usually ignored result in hundreds of spurious excesses. Both catalogues have various quantities that can be used to identify and mitigate these problems. These are either flags that indicate contamination, saturation, upper limits, etc., or values that quantify some property such as the goodness of fit achieved in the source extraction. Most issues were uncovered in early SED fitting runs, where the distribution of some catalogue property (source extraction quality for example) was very different for excesses than for the bulk population.

The WISE catalogue has several indicators that can be used to remove suspect photometry, which are related to either source

extraction or image artefacts.⁶ We first consider the reduced χ^2 from the source extraction for each WISE bands, whose distributions are shown in Figure 3 (the columns in the catalogue are called $wXrchi2$ where X is 1, 2, 3, or 4). These measure the quality of the profile fitting source extraction; a high value is a likely indicator that the source is not well described by a point source, so could be resolved or confused with another object. Any deviation from a point source cannot be due to a resolved debris disk; most *Kepler* stars are hundreds to thousands of parsecs away and WISE is sensitive to warm excesses that lie at small stellocentric distances (i.e. have very small angular size)

The most noticeable feature in Figure 3 is that W1 shows a non-Gaussian distribution. Given that the difference in beam FWHM from W1 to W2 is only $6''.1$ vs. $6''.4$ and the wavelength difference is small, it seems unlikely that such a large difference in the χ^2 distributions is astrophysical. However, we found that sources with poor W1 source extraction were more likely to show excesses (above $w1rchi2$ of about 2), which we attribute to confusion with nearby sources. Based on this result and the distributions in Figure 3 we avoid poor source extraction by keeping WISE photometry only when the χ^2 is smaller than 2, 1.5, 1.2, and 1.2 in W1-4 respectively. A similar, but less stringent cut is also made by only retaining sources where the extension flag (`ext_flg`) is zero, which means that no band has a $\chi^2 > 3$ and the source is not within $5''$ of a 2MASS Extended Source Catalogue entry.

The WISE catalogue also provides flags (the `cc_flags` column) that note contamination from diffraction, persistence, halo, and ghost artefacts. These flags indicate the estimated seriousness of the contamination; whether the artefact may be affecting a real source, or the artefact may be masquerading as a source. We avoid photometry with any indication of contamination (i.e. both types).

Applying these quality criteria to the WISE data results in 126743, 128610, 78340, and 9790 detections with a signal to noise ratio of greater than three in W1-4 respectively. A total of 144655 sources have a WISE detection in at least one band.

The 2MASS catalogue also has columns for the profile fitting source extraction χ^2 in each band (called $J, H, Kpsfchi$).⁷ Early SED fitting runs found that nearly half of the W1-2 excesses had a 2MASS reduced $\chi^2 > 2$, particularly in the J band. Given that only about 5% of all 2MASS sources matched with KOBs have a J band $\chi^2 > 2$, we concluded that the higher W1 and W2 excess occurrence rate was related to the poorer 2MASS source extraction. As with the WISE W1 source extraction we attribute this correlation to confusion. We therefore only use 2MASS data when the χ^2 from source extraction for all three bands is less than 2.

We exclude 2MASS photometry for about 5,000 2MASS objects that have the E, F, X, or U photometric quality flags. The first two flags represent the poorest quality photometry, the third is for detections for which no brightness estimate could be made, and the last is for upper limits.

We also used early SED fitting runs to assess the quality of the photometry in each band. We found that Tycho 2 photometry is poorly suited to the task at hand. While the measurements appear accurate, only a few thousand KOBs are brighter than about 11th magnitude ([Batalha et al. 2010](#)), and objects fainter than this have large Tycho 2 uncertainties (see [Høg et al. 2000](#)). Because most KOBs are near or beyond the Tycho 2 magnitude limits, their precision is poor and we did not use this photometry.

⁶ http://wise2.ipac.caltech.edu/docs/release/allsky/expsup/sec2_2a.html

⁷ http://www.ipac.caltech.edu/2mass/releases/allsky/doc/sec4_4b.html

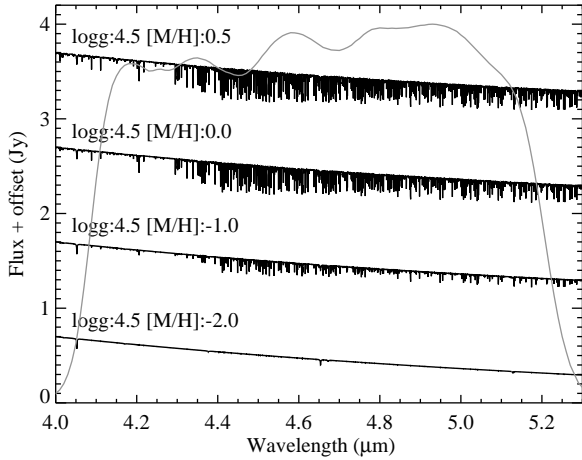


Figure 4. Metallicity-dependent absorption in the W2 band for $\log g = 4.5$ and a range of $[M/H]$ for a Solar-type star. The W2 bandpass is also shown (arbitrary units, grey line).

Finally, we found that the KIC u photometry was commonly offset below the photospheric models. Given that only 1092 stars have u photometry we also excluded this band from the fitting.

3.1.2 W2 absorption

The W2 band lies on top of the fundamental CO bandhead, whose depth varies strongly with metallicity for the bulk of our sample. This effect is shown in Figure 4, where the lines of model spectra within the W2 bandpass (grey line) become deeper with increasing metallicity. In this plot the flux at the W2 isophotal wavelength varies by 10% between $[M/H]$ of -2 to +0.5.

As the metallicity increases, the spectrum changes and the colour correction that should be applied to the catalogue (sometimes called “quoted”) flux also increases. Commonly, IR colour corrections are simply taken to be those for a blackbody at the stellar effective temperature. With this approach the examples in Figure 4 would all have the same colour correction. Thus, inaccuracies in the derived metallicities would lead to a (spurious) trend of larger W2 excesses for more metal rich stars. However, when computed properly the colour correction increases with the level of absorption by a similar amount (see also [Wright et al. 2010](#)). That is, in the metallicity range considered at 5800K, the actual fluxes vary by about 10% but the quoted fluxes vary by only 1%. WISE is therefore not actually very sensitive to metallicity for Sun-like stars. This sensitivity depends on effective temperature and is strongest for M dwarfs. This conclusion is borne out by the analysis in §3.2 below.

3.1.3 Final photospheric models

The final SED models are generated based on the conclusions of this section. These were computed for all but five of the WISE matches (that have no reliable photometry and are identified in the KIC as galaxies). With the photospheric predictions in the W2-4 bands made based on the optical and near-IR photometry, we now look for excesses.

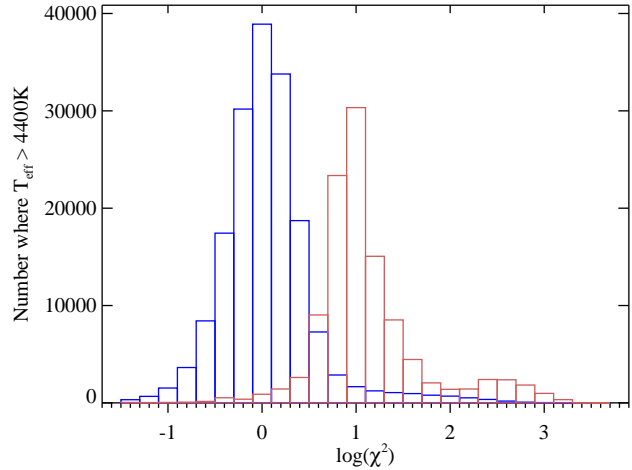


Figure 5. SED reduced χ^2 for stars hotter (filled bars) and cooler (empty bars) than 4400K (number multiplied by 14). Cooler stars clearly have poorer fits, due either to missing opacity or incorrect bandpasses.

3.2 Selecting stars with excesses

With a complete set of SEDs, the task of finding excesses is in principle very simple; stars with excesses greater than a sensible significance threshold are selected. In practise this step is complicated by several factors. Atmospheric models for M dwarfs are known to overestimate the stellar flux in the Rayleigh-Jeans regime (e.g. [Lawler et al. 2009](#)). Some stars have poor fits and many of these result in excesses that are not real and should be excluded. The sample also contains many giants, whose excesses may be attributed to mass loss rather than a debris disk.

In our sample, there is a clear transition in the quality of the SED fits around 4400K. Stars cooler than this value have consistently poorer fits than those that are hotter. Such a trend may be due to missing opacity in the stellar atmospheres, but could also be caused by poor filter characterisation. Figure 5 shows χ^2 histograms for the SED fitting, where χ^2 is the reduced sum of squared differences between the photometry and the photospheric model. When split by effective temperature at 4400K there is a clear difference between the two sets, so we apply a different cut in χ^2 for each; for stars hotter than 4400K we keep stars with $\chi^2 < 10$, for those cooler than 4400K we keep stars with $\chi^2 < 100$. We do not simply ignore these cool stars, because the photospheric predictions are generally reliable (though not always, as we find in §4.1).

Having made this cut in the quality of the SED fits, Figure 6 shows the excess significance for bands W1-4. Though we have included W1 in the photospheric fitting, if the photometry in the shorter wavelength bands is of high quality then W1 will still show an excess if present. The dot colours indicate the gravity derived for the KIC (and used by us with the offset noted above), and show that some W3-4 excesses are present around stars with lower gravities (i.e. bluer dots around brighter stars with excess significance above 3-4). We therefore remove giants using the criteria of [Ciardi et al. \(2011\)](#), where a star with $T_{\text{eff}} > 6000$ is assumed to be a giant if $\log g < 3.5$ and a star with $T_{\text{eff}} < 4250$ is assumed to be a giant if $\log g < 4.0$, with a linear transition for intermediate temperatures. Because we have adjusted the gravity of giants as derived in the KIC, we likewise shift their giant criterion down accordingly so our criterion selects the same stars.

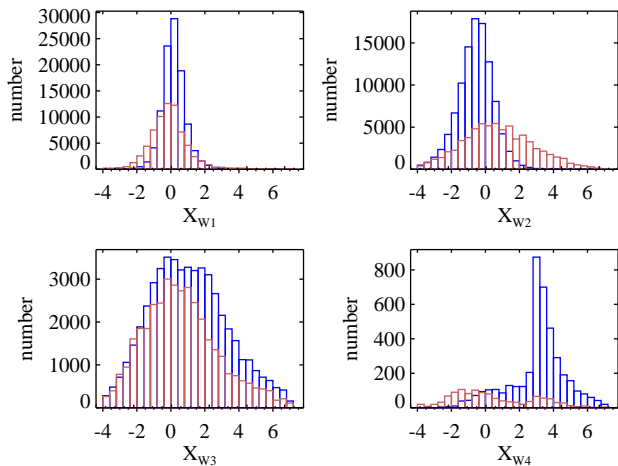


Figure 7. Excess significance histograms for the W1-4 bands for stars hotter (filled bars) and cooler (empty bars, number multiplied by 15, 15, 10, and 1 respectively) than 4400K.

A feature present in Figure 6 for the W3-4 bands is a flux-dependent cut-off below about 0.5 and 5mJy respectively. This cut-off is simply the WISE sensitivity limit, which shows that the faintest stars can only be detected if the W3-4 flux is greater than the photosphere (due to statistical variation or real excess emission).

Having removed poor SED fits and giants, the remaining task in identifying excesses is to set the threshold level of significance. Normally this level would be around 3-4 if the uncertainties are estimated appropriately, but there are a very large number of W3 excesses above this level. Figure 7 shows the significance distributions, and W3 clearly has many excesses that would be considered significant (as does W4, but to a lesser degree). These cannot be debris disks, because the excesses that WISE can detect around *Kepler* stars are rare. The distribution should therefore appear largely Gaussian with a dispersion of unity, with only a few objects at higher positive significance. Aside from being affected by sensitivity limits as seen for W3-4, the negative side of the histogram should be Gaussian (i.e. negative excesses cannot arise, even if positive excesses arise due to true astrophysical phenomena), and the extent can be used to estimate a reasonable significance threshold. Because the histograms do not show negative excesses below a significance of -4 , we set the threshold at $+4$ for W1-4, and address the origin of the large number of excesses below.

We make an exception to this threshold for W2 excesses around cooler stars. The significance distribution for W2 is much wider than for hotter stars and skewed to larger values (Fig. 7). This difference presumably arises due to greater absorption in the W2 band (see §3.1.2). Plotting the significance against metallicity indeed shows a strong correlation, which could either be a sign that W2 excesses around M stars are strongly correlated with metallicity or that the metallicity of these stars in the KIC is too high (i.e. the absorption in the model is stronger than in reality). Given that debris disks around nearby M dwarfs appear to be very rare (Lestrade et al. 2006; Gautier et al. 2007; Lestrade et al. 2009) and show no such trend, the latter is the more sensible conclusion and we set the significance threshold at 7.

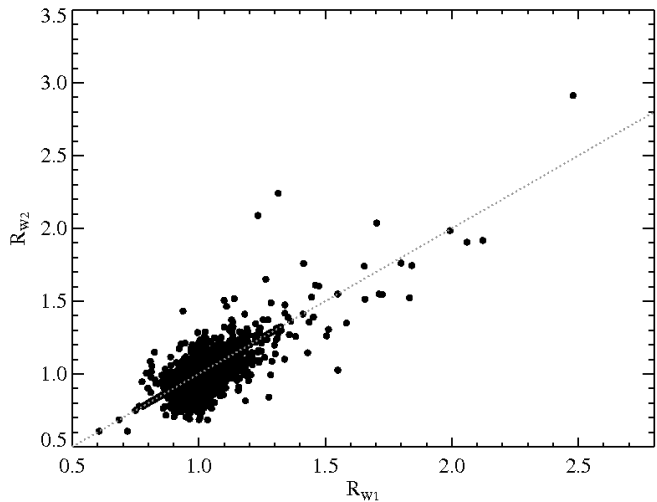


Figure 8. Flux ratios in the W1 and W2 bands compared for all stars with excesses (the dotted line is $y = x$, not a fit to the data). The strong correlation is not expected for dust emission and is due to poor photospheric predictions.

4 INTERPRETATION OF EXCESSES

With our chosen significance criteria, there are 7,965 disk candidates. There are 79, 95, 7480, and 1093 excesses in bands W1-4 respectively. These excesses correspond to an occurrence rate of about 4%. Since about 4% of nearby Sun-like stars have $24\mu\text{m}$ excesses (e.g. Trilling et al. 2008) from calibration limited observations (flux ratios $\gtrsim 1.05$), the finding of a similar rate from much less sensitive WISE observations (see Fig. 2) indicates that unless the stars observed by *Kepler* are somehow unique, most of the excesses cannot be due to debris. We therefore take a closer look at the origins of these excesses in the next two subsections. In what follows, we group stars into three effective temperature bins; “M-type” ($T_{\text{eff}} < 4400\text{K}$), “FGK-type” or “Sun-like” ($4400 < T_{\text{eff}} < 7000\text{K}$), and “A-type” ($7000 < T_{\text{eff}} < 10,000\text{K}$). Only ten excesses are found for stars hotter than 10,000K, all in W3, and none survive the following analysis.

4.1 W1-2 excesses: poor photospheric predictions

A handful of targets show W1-2 excesses, but Figure 8 argues that they are probably not due to circumstellar debris. Plotting the flux ratios in the W1 and W2 bands shows that these quantities are correlated, with a slope of approximately unity. The excess can therefore be accounted for by shifting the stellar spectrum upward.

Inspection shows that the objects with the largest ($\gtrsim 1.5$) flux ratios in W1-2 are the result of failed photospheric fits, where the optical photometry is at odds with the WISE photometry. In these cases the stellar temperature is generally below 4400K, and were not cut due to the relaxed photospheric fit χ^2 for these objects. These objects typically have no temperature in the KIC, meaning that no reasonable fit could be found there either.

Some objects have smaller flux ratios in W1-2 that are also significant, but these ratios remain well correlated. While some are still due to poor photospheric predictions, another explanation is that the W1-2 photometry includes two stars. The excess flux in the W1-2 bands could be caused by the emission from a cooler star that lies within the instrumental PSFs of all photometry (and may

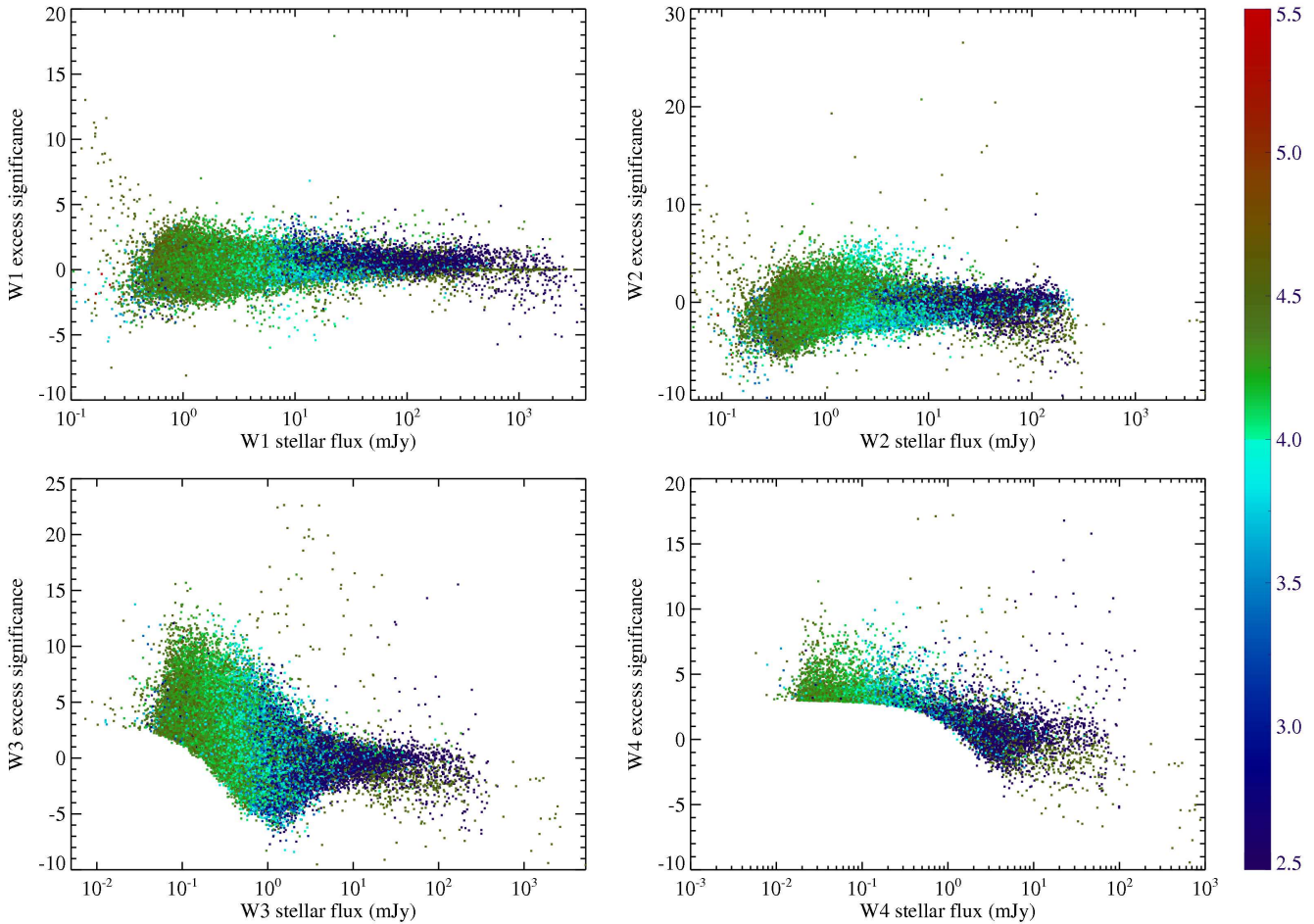


Figure 6. Excess significance vs. predicted photospheric flux in the W1-4 bands. The colour scale is $\log g$. Any object with significance greater than 3-4 plausibly has a real excess.

or may not be associated with the *Kepler* star in question). It is also possible that the higher resolution 2MASS and optical photometry used to predict the photosphere measured flux from one of a pair of stars, while WISE measured flux from both. Such a situation can also lead to identification of an excess where there is none.⁸

Based on the strong correlation between the flux ratios in W1 and W2, we conclude that while some excesses are likely real in that the spectrum departs from our model of a single stellar photosphere, it is unlikely that any are excesses are due to circumstellar dust.

4.2 W3-4 excesses: disks or background?

While we have taken care to remove spurious detections (see §3.1.1), the WISE sensitivity and resolution and the very large sample size mean that extra-Galactic contamination due to chance alignments, even at very low levels, could contribute to, or even be

the cause of, the W3-4 excess population. Further, the low Galactic latitude of the *Kepler* field means that IR flux levels from dust within our Galaxy can be significant (see Fig. 1).

4.2.1 Galactic background contamination

The hypothesis that the Galactic background level is the cause of the very large number of W3 excesses can be tested by simply plotting their locations on the sky, shown as dots in Figure 9. The excesses clearly reside in clumps, and appear more frequent closer to the Galactic plane. Therefore, the bulk of the W3 excesses are likely spurious.

To remove these false excesses in a way unbiased for or against the presence of excess emission therefore requires ignoring excesses in the highest background regions. Ideally this cut would be made based on the WISE catalogue itself. In general however, the background (`w3sky` column in the catalogue) is smooth, and shows no relation to the clumpiness seen for excesses except very near to the Galactic plane. This smoothness is perhaps a result of the dynamic WISE calibration, which attempts to remove temporal

⁸ An example is HIP 13642, identified by Koerner et al. (2010) as an excess because the MIPS observation includes two stars, while the 2MASS observation used to predict the photosphere resolves the pair.

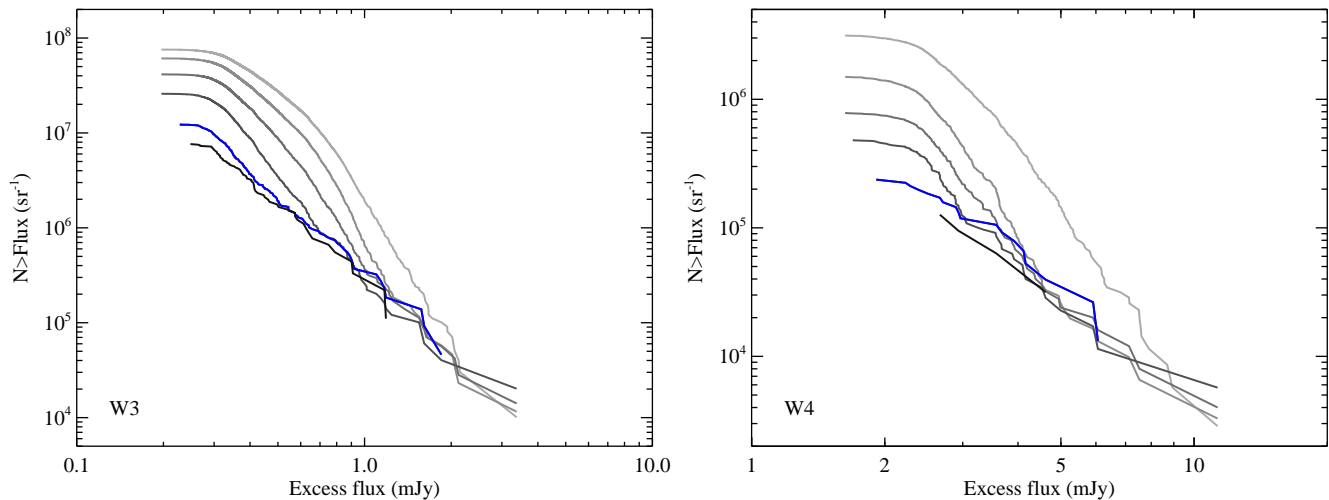


Figure 10. Cumulative source counts in W3 (left panel) and W4 (right panel). The solid lines show the counts for excesses as the cut in IRAS $100\mu\text{m}$ background flux is increased. The lines show no cut (top line), and then levels of 15, 10, 7, 5, and 4 MJy/sr. As the cut in IRAS background increases the excess counts approach a fixed level, indicating that the remaining excesses are not caused by Galactic background emission. The blue line shows our adopted cut level of 5 MJy/sr.

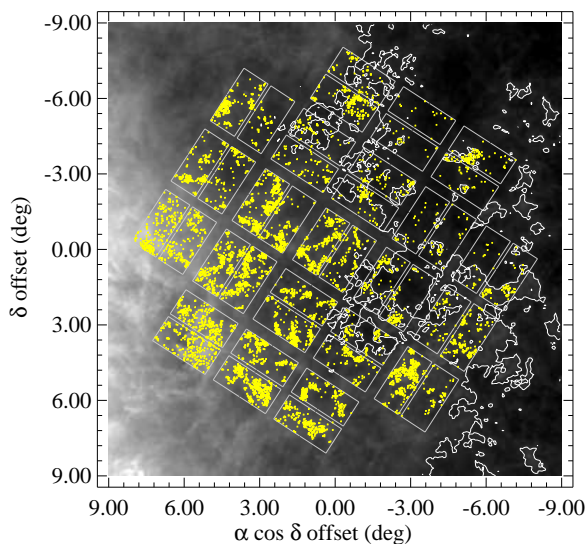


Figure 9. Clumping of stars with W3 excesses (yellow dots) indicating that the excesses are due to the high background level. The 5 MJy/sr cut based on the IRAS $100\mu\text{m}$ background image is shown by the white contours.

instrumental variations.⁹ We found that instead the $100\mu\text{m}$ IRAS IRIS map is a very good indicator of the background level, which we use to exclude sources below.

Figure 10 shows how the cumulative number of excesses changes as a function of the IRAS background level. To make the plots comparable with those below, we scale the number of excesses by dividing by the area covered by the WISE observations. We take the observed area for a single star to be that enclosed by a circle whose diameter is the WISE point spread function (PSF)

⁹ http://wise2.ipac.caltech.edu/docs/release/allsky/expsup/sec4_4a.html

full-width at half-maximum (FWHM, $6''.5$ and $12''$ for W3-4 respectively). These areas are multiplied by the number of non-giant stars with satisfactory SED fits that were observed and lie in regions below the given background level (and for which photometry was not removed for any of the reasons in §3.1.1).

In each plot the highest line shows the full set of excess counts. The lower lines show how the excess counts decrease as an increasing cut in the IRAS $100\mu\text{m}$ background level is made. Once the cut level reaches about 5 MJy/sr the excess counts stop decreasing, indicating that the excesses that are due to the high background level have been removed. Higher cut levels do not decrease the distributions further and simply result in fewer remaining excesses.

The region where the IRAS background level is lower than 5 MJy/sr is shown in Figure 9. The contours mark out and avoid regions where excesses clump together well. Based on this approach, we conclude that 5 MJy/sr is a reasonable cut level to avoid contamination from the high Galactic background level. Of the initial 7,965 disk candidates, 271 remain after this cut.

4.2.2 Extra-Galactic counts

The remaining 271 excesses are generally real in the sense that they arise from point-like flux above the photospheric emission at the location of the *Kepler* stars. However, we now test whether these could arise from chance alignments with background galaxies. To estimate the number of excesses expected from extra-Galactic contamination we therefore first derive galaxy counts specific to our sample. The galaxy counts are derived by counting the number of sources above a given flux at a given wavelength after the contribution of Galactic stars has been removed.

Because galaxy counts may be subject to cosmic variance, and could appear to be different in the *Kepler* field due to stellar crowding and a relatively high background level near the Galactic plane, we show the results from several different fields and surveys in Figure 11. For comparison with WISE W3 we show $15\mu\text{m}$ ISO results (La Franca et al. 2004) and for W4 we show $24\mu\text{m}$ *Spitzer* MIPS results (Papovich et al. 2004; Clements et al. 2011). We compare these with counts from two fields we extracted from the WISE cat-

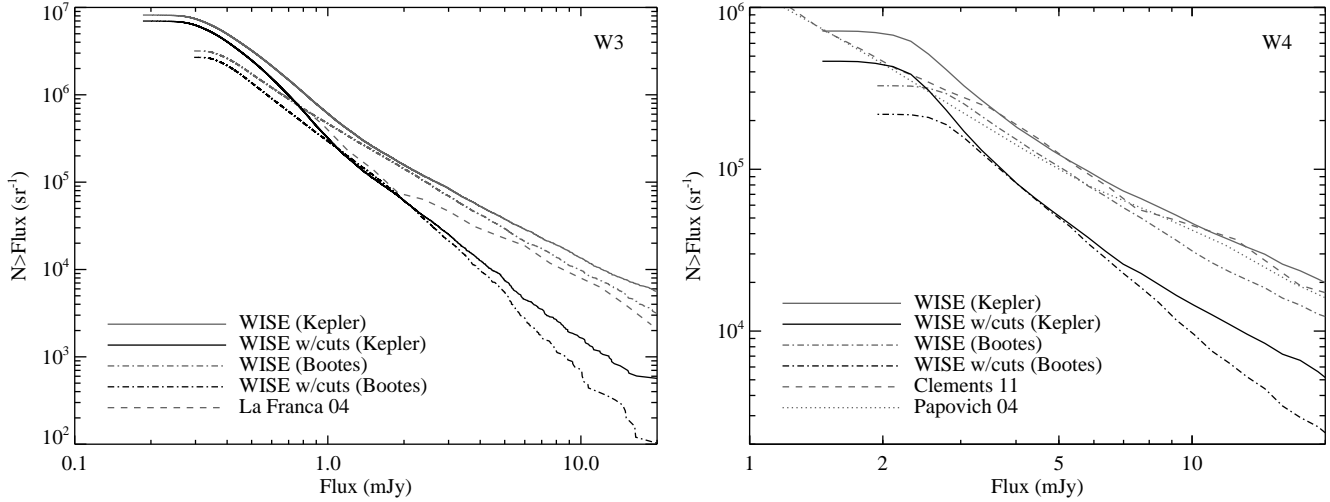


Figure 11. Comparison of cumulative galaxy source counts in W3 (left panel) and W4 (right panel). The grey lines show galaxy counts from ISOCAM at $15\mu\text{m}$ (left panel, [La Franca et al. 2004](#)) and *Spitzer* MIPS at $24\mu\text{m}$ (right panel, [Papovich et al. 2004](#)), and from WISE in two different fields (see text). The black lines show the same WISE fields, but with the additional cuts outlined in §3.1.1 (i.e. the same cuts as were applied in our search for excesses around *Kepler* stars).

ologue. The first is a box in the *Kepler* field between $286\text{--}296^\circ$ right ascension and $40\text{--}50^\circ$ declination (71 square degrees). The second is a “random” box farther away from the Galactic plane in Boötes, between $210\text{--}220^\circ$ right ascension and $30\text{--}40^\circ$ declination (82 square degrees, at a Galactic latitude of about 70°).

For our analysis of the WISE data we require A, B, or C quality photometry (`ph_qual`), and $S/N > 4$, and remove the stellar contribution by keeping sources with $W1 - W3, 4 > 1.2$ (see [Jarrett et al. 2011](#)). These source counts are shown in Figure 11 in grey, and follow the ISO and *Spitzer* counts well. The agreement suggests that cosmic variance is not significant for these fields (i.e. the distribution of background galaxies is similar in the *Kepler* field to elsewhere). The WISE counts are similar for both fields, though the *Kepler* field shows somewhat increased counts at the lowest flux levels.

We then add the cuts outlined in §3.1.1, which were made with the intention of minimising galaxy contamination, for which the results are shown as black lines. The black lines lie below the grey ones, indicating that the extra cuts do indeed remove some galaxies. The cuts are more effective in W4 with an overall decrease, while at W3 the cuts are only effective for brighter galaxies. Because we want to quantify the extra-Galactic contribution to our excesses, we use the black line from the *Kepler* field as the expected level of galaxy contamination.

4.2.3 Extra-Galactic contamination

We now proceed with the remaining excesses where the IRAS $100\mu\text{m}$ background is lower than 5MJy/sr (listed in Table 1). The comparison of these excesses (again expressed as counts per sky area) and the galaxy counts derived above is shown in Figure 12, where we have now separated the excesses by spectral type. In these plots, the galaxy counts do not move. The excess counts from disks depend on their occurrence rate and the distance to the stellar sample. Naturally, a higher disk fraction would move the excess counts upward on this plot, away from the galaxy counts, and the chance of an individual excess being due to a background galaxy would be lower. For a fixed excess distribution, samples of stars that are on

average fainter and brighter (i.e. farther and nearer), move the excess count lines left and right respectively. Thus, the excess counts from disks for samples of brighter stars lie higher above the galaxy counts than samples of fainter stars, and again the likelihood of contamination is lower. This advantage arises because for fixed disk to star flux ratio (i.e. fixed disk properties), the absolute flux from a debris disk around a bright star is more than that from a faint star. At brighter flux levels the number of galaxies per unit sky area is smaller, so the likelihood of confusion lower. Finally, higher instrument resolution means less chance of confusion with a background galaxy because the area surveyed per star is smaller. Therefore, the same population of excesses observed with a larger telescope would also be further above the galaxy counts and more robust to confusion.

In Figure 12, we make one additional cut to the number of stars that count towards the total area observed, by only including stars whose photospheres are equal to or brighter than that of the faintest star found to have an excesses. This photospheric flux cut makes use of the fact noted above, that brighter stars are more robust to confusion (assuming that the presence or otherwise of a disk is independent of stellar brightness for fixed spectral type). This cut has little effect for most excesses because the faintest star with an excess is near the limit for all stars. However, it is effective for the W4 excess associated with an A-type star because this star is brighter than the bulk of the sample. In W3 the total number of non-giant stars that survive the cut in background level is 1198, 24916, and 1462 for M, FGK, and A stars respectively. In W4 the numbers are 750, 23742 and 10 for M, FGK and A-types. The very small number of A-type stars as bright or brighter than the one with an excess shows why the cut in photospheric flux is useful.

For W3 (left panel of Fig. 12) the excess counts for 19 M-type, 235 Sun-like and 11 A-type stars lie very close to the counts expected from background galaxies. Thus, not many, if any, of the excesses appear attributable to debris disk emission. The disk occurrence rate is insufficient to allow detection of debris disks that are robust to galaxy confusion (e.g. have a less than 1/10 chance of being a galaxy). The single *Kepler* planet host candidate (*Kepler* Object of Interest, or KOI) found to have an excess ((KOI 861 a.k.a.

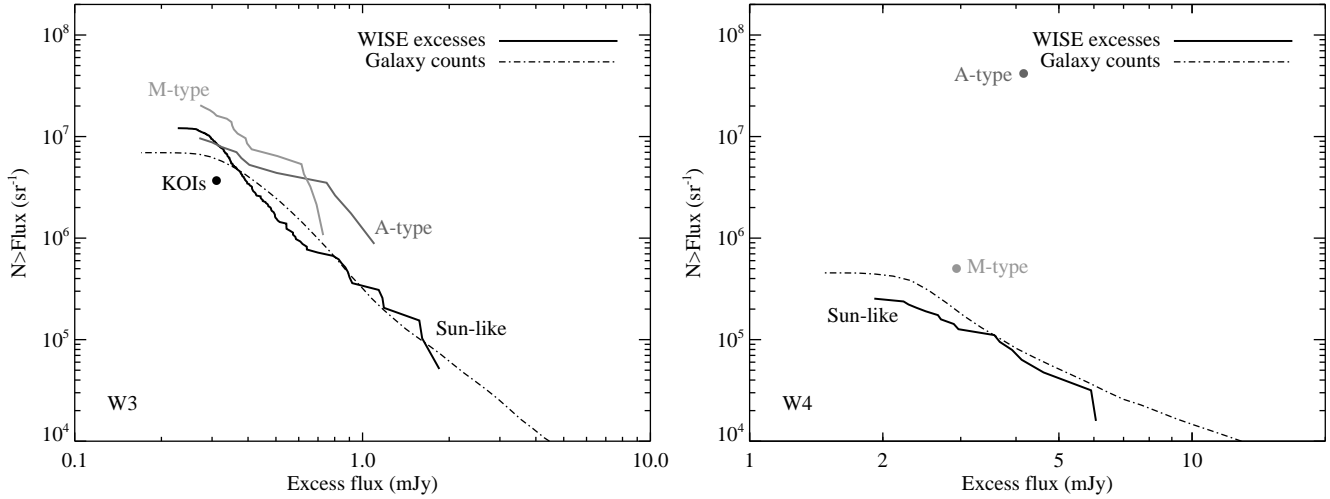


Figure 12. Cumulative source counts in W3 (left panel) and W4 (right panel). The solid lines shows the counts for excesses, split into M-type, Sun-like and A-type (there are no W4 excesses around M-types). The dot-dashed line shows our WISE counts in the *Kepler* field (solid lines in Fig. 11). The dot is the single planet host candidate found to have an excess (KOI 861). All excesses lie near the level expected from background galaxies, with the exception of a single W4 excess around a nearby A-type stars.

Table 1. The 271 *Kepler* stars with WISE 3-4 excesses (full table in the appendix of this arXiv version). Columns are: KIC identifier, predicted *Kepler* (K_p) magnitude from the KIC, Quarters the star was observed in (up to 6), fitted effective temperature, W3-4 flux ratio and excess significance (where $X_{W3,4} \geq 4$). The note column notes the single KOI, and potential planet hosts from Tenenbaum et al. (2012) (“T12”).

KIC	K_p	Quarters	T_{eff}	R_{W3}	X_{W3}	R_{W4}	X_{W4}	Notes
5866211	15.19	456	6585	4.2	5.0			
5866341	15.06	123456	6296	4.9	6.7			
5866415	15.33	123	6029	4.7	4.4			
6198278	14.86	123456	5436	2.8	4.1			
6346886	14.96	12346	5869	3.9	4.6			
6431431	14.87	123456	8147	5.9	7.8			
6503763	15.78	12346	5275	4.3	4.1			
6515382	13.29	123456	6265	1.7	4.2			
6516101	13.88	123456	6062	2.3	6.1			
6599949	15.42	123456	5773	4.0	4.1			
6676683	14.58	123456	6356	4.1	6.2			
6685526	15.00	123456	5103	2.7	4.1			KOI 861,T12

KIC 6685526, Borucki et al. 2011; Batalha et al. 2012) is shown as a single point, as one of 348 KOIs that survive the IRAS background cut. It lies very close to the A, FGK, and M-type sample counts, so is equally likely to be confused. Because the excesses are heavily contaminated, the excess distributions represent an upper limit on the distribution of W3 excesses (we return to these limits in §§5.3 and 6).

For W4 (right panel of Fig. 12) the 16 Sun-like excess counts lie slightly below the galaxy counts, the single M-type excess slightly above, while the single A-type excess lies well above. Because galaxy counts are independent of stellar spectral type, there should be no difference between the contamination level for M-type, Sun-like and A-type stars. Therefore, the $22\mu\text{m}$ A-type excess, which has a moderate $22\mu\text{m}$ flux ratio of 1.63, is very likely due to debris disk emission. Because the difference between the A-type excess counts and the WISE galaxy counts is about a factor of one hundred, there is about a 1/100 chance that this A-star excess is a galaxy. It is likely that all Sun-like W4 excesses and the single M-type excess can be explained as galaxy confusion, so again the disk occurrence rate is too low to allow robust disk detection and the excess counts represent an upper limit.

It is perhaps surprising that the excess and galaxy counts in Figure 12 agree as well as they do. The galaxy counts were derived from all sources that met certain criteria within a specific patch of sky with the assumption that confusion only happens within the WISE PSF FWHM, while the excess counts were the result of the SED fitting method using WISE photometry at positions of known stars. We applied a cut in the background level to remove spurious excesses, but no such cut was required for the galaxy counts. The extra-Galactic counts in the *Kepler* field agree well with those for the Boötes field, where the IRAS $100\mu\text{m}$ background level never reaches more than about 3MJy/sr (i.e. is always below our cut in background level), so the extra-Galactic counts in the *Kepler* field are relatively unaffected by the background. Therefore, there appears to be a preference for stars (which are almost always detected in W1-2) to show a spurious W3-4 flux due to high background levels, while galaxies (which are generally not detected in W1-2) do not. This difference may be attributed to the WISE method of source extraction, which attempts to measure fluxes across all four bands if a source is detected in at least one.

4.3 Comparison with previous results

Our study is not the first to use WISE to look for warm emission from disks around *Kepler* stars (Ribas et al. 2012; Lawler & Gladman 2012). Ribas et al. (2012) found 13 candidate disk systems using the WISE preliminary release, 12 of which are observed by *Kepler* (the other is WASP-46, a nearby system with a transiting planet, Anderson et al. 2012). However, they use an excess significance threshold of 2 (see eq. 3). At this level 2.3% of systems are expected to have significant excesses purely due to the fact that the uncertainties have a distribution (that is assumed to be Gaussian). Therefore, of the 468 *Kepler* planet host candidates they considered, 11 should lie above this threshold. This number is similar to their 12 disk candidates, so these candidates are consistent with being part of the expected significance distribution if no stars have disks.

Three of their twelve disk candidates have significance higher than 3, but all lie in regions where the $100\mu\text{m}$ background is higher than 5MJy/sr so are excluded from our analysis because their excesses are likely due to the high background level (§4.2.1).¹⁰

In contrast to our conclusions, Ribas et al. (2012) find that background contamination is negligible, with a 5×10^{-5} chance of a galaxy brighter than 5mJy appearing within $10''$ of a source at $24\mu\text{m}$, using counts from Papovich et al. (2004). However, these counts show about 10^5sr^{-1} for sources brighter than 5mJy (see Fig. 11), so a target area of 314 square arcseconds ($10''$ radius) yields $10^5 \times 314 \times 2.35 \times 10^{-11} = 0.001$ probability of having a 5mJy background source within $10''$ of a target. However, the WISE beam is in fact smaller than $10''$ radius, so using $6''$ is more appropriate (see previous subsection). Furthermore, removing WISE photometry that is flagged as extended decreases the W4 counts (Fig. 11), so the Papovich et al. (2004) counts overestimate the confusion level that applies here by a factor of about two. Therefore, 0.06 spurious excesses are expected from 468 targets. This expectation is in line with the two sources they report with W4 excesses, KIC 2853093 and KIC 6665695, since these have W4 S/N of 2.2 and 2.5 respectively and as noted above we would not consider these significant given the sample size.

All of their candidates have $12\mu\text{m}$ excesses, so should be compared with galaxy counts at a similar wavelength (e.g. $15\mu\text{m}$ ISO counts). Based on Figure 11, about 5×10^6 background galaxies per steradian are expected down to the detection limit of about 3mJy , which for a target radius of $3.25''$ (33 square arcseconds) yields an expected contamination rate of $5 \times 10^6 \times 33 \times 2.35 \times 10^{-11} = 0.004$. Thus, about 2 spurious excesses among 468 targets is expected at this wavelength. Of their W3 disk candidates, three have excesses more than 3σ significant. However, KOI 1099 has W3-4 upper limits in the newer all-sky release, so the expectation of two spurious excesses appears to be met. Both sources lie in the regions we excluded due to the high background so the WISE photometry may still be spurious.

In a similar study, Lawler & Gladman (2012) reported the discovery of excess emission around eight *Kepler* planet-host stars using the WISE Preliminary release. They used a significance criterion of 5σ , so their excesses should be astrophysical (i.e. not statistical). There are only three candidates in common with Ribas et al.

¹⁰ KOI 469 has a very bright moving object (i.e. an asteroid or comet) visible in the WISE images at a separation of about 6 arcminutes, which may have affected the source extraction. Given the rarity of excesses, it seems more likely that the apparent excess is due to the presence of the bright object, rather than coincidental.

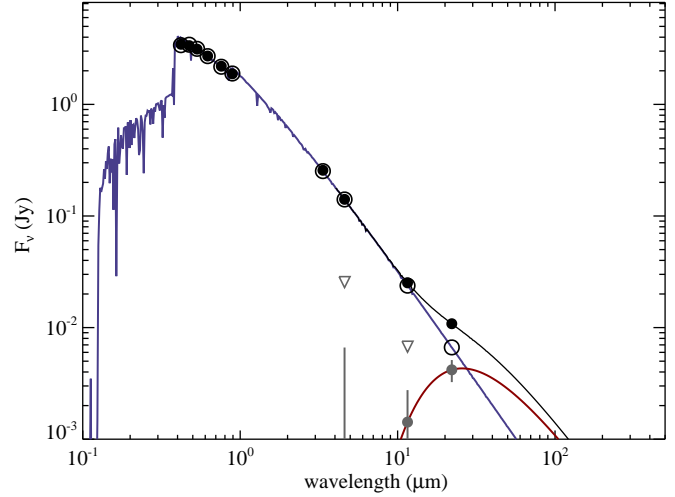


Figure 13. SED for the A-type W4 debris disk candidate KIC 7345479. The stellar spectrum is shown in blue, and the fitted blackbody in red. The sum of the two is shown in black. KIC and WISE photometry is shown as black dots, and synthetic photometry of the star in the same bands as open circles. Grey symbols show the star-subtracted fluxes, with a triangle above indicating the 4σ upper limit if necessary.

(2012). However, these are the three noted above with a significance greater than 3σ , so Lawler & Gladman (2012) find the same candidates as Ribas et al. (2012) with an additional five disk candidates. Of their eight, the WISE W3 and W4 measurements of KOI 904 and KOI 1099 are upper limits in the newer all-sky WISE catalogue, and KOIs 871, 943, 1020, and 1564 were rejected by Ribas et al. (2012) after image inspection. The same two plausible disk candidates remain, corresponding to the number estimated above to arise from confusion. Though the details vary, these two studies are basically consistent if a $3\text{-}5\sigma$ significance criterion is used and candidates are rejected based on the images.

4.4 Debris disk candidate

We now briefly outline some properties of our most promising disk candidate, KIC 7345479 (with a *Kepler* K_p magnitude of 7.9), shown in Figure 13. Assuming that this star is a dwarf yields a distance of 280pc , much closer than most *Kepler* stars. The SED shows the 9700K stellar spectrum, along with a simple blackbody fit to the excess that includes the W2-4 photometry. With a measured flux of $10.8 \pm 0.9\text{mJy}$ and a photospheric flux of $6.6 \pm 0.2\text{mJy}$ the W4 excess has a flux ratio $R_{W4} = 1.6$, with significance $X_{W4} = 4.5$. The disk temperature is constrained by the W3 upper limit, so is cooler than about 200K , corresponding to a radial distance of greater than 15AU and lies beyond the region of *Kepler* sensitivity to transiting planets. The fractional luminosity for the blackbody model shown is 3.25×10^{-5} . As we show in §5 below, aside from the potential for planet discovery around the host star, this disk is fairly unremarkable within the context of what is known about disks around nearby A-stars.

5 NEARBY STAR COMPARISON

There should be nothing particularly special about *Kepler* stars compared to nearby stars, so we compare our survey with $24\mu\text{m}$

results from two large unbiased *Spitzer* surveys of nearby stars. Because the results can only be interpreted within the context of what was possible with each survey, we first compare the sensitivity to disks for the *Spitzer* surveys in the fractional luminosity vs. temperature space introduced in Figure 2. We also make a brief comparison with IRAS results at $12\mu\text{m}$.

5.1 Disk sensitivity at 22-24 μm

The left panels of Figure 14 show the sensitivity to disks with WISE at $22\mu\text{m}$, split into Sun-like and A-type stars. The plots are similar to Figure 2, but now represent the cumulative sensitivity for all objects. Disks in the white region could have been detected around all stars, and disks in the black region could not have been detected around any star.

For the Sun-like *Kepler* stars observed with WISE (top left panel), the region covered for the bulk of the stars is similar to that predicted in Figure 2. Only the brightest few stars have sensitivity to fractional luminosities lower than about 0.1%. No disks are shown on this plot because the W4 excesses around Sun-like stars are consistent with arising entirely from background galaxies.

The WISE sensitivity is in contrast to that for nearby Sun-like stars observed with *Spitzer* at $24\mu\text{m}$ (top right panel, Trilling et al. 2008), which could detect disks with much lower fractional luminosities (i.e. the white region extends to lower f). The WISE sensitivity does not extend into the region where disks were detected with *Spitzer*, so does not probe the same part of the disk distribution as the *Spitzer* study.

Compared to nearby A-stars observed with *Spitzer* (lower right panel), the disk and lowest contours for WISE extend into the region covered by the brightest excesses found by Su et al. (2006) (i.e. where $T_{\text{disk}} \sim 100\text{-}200\text{K}$ and $f \sim 10^{-3}\text{-}10^{-4}$). Unlike the Sun-like stars, there is therefore some overlap in the parts of the disk distributions that are detectable with each survey. For the WISE A-star disk candidate (dot in lower left panel) we assume the disk properties shown in Figure 13. Because this temperature is an approximate upper limit, the disk could lie anywhere along the white line that curves towards the upper left of the figure (though cooler disks must have significantly higher fractional luminosities). The WISE detection is very likely typical based on where it lies relative to the known distribution of A-star excesses.

5.2 Excess distribution at 22-24 μm

Figure 15 shows cumulative 22 and $24\mu\text{m}$ flux ratio distributions, again split into Sun-like and A-type samples. The nearby star distributions are simply the cumulative distribution of flux ratios, since all observed stars were detected.

For Sun-like stars (left panel), because we concluded that all W4 Sun-like excesses were consistent with arising from contamination by background galaxies (§4.2, Fig. 12), the WISE part of the distribution is an upper limit on the occurrence rate of rare bright disks. It is found by assuming upper limits on flux ratios are detections (i.e. by assuming that all stars could have disks just below detectable levels, whereas the true distribution lies somewhere below this level). The lack of overlap in the distributions due to the rarity of large 22-24 μm excesses, and the limitations of WISE observations of *Kepler* stars, is clear.

While lower levels of excess (flux ratios of $\sim 1.1\text{-}2$), have an occurrence rate of around 2-4% around Sun-like stars (e.g. Fig. 15, Hines et al. 2006; Beichman et al. 2006b), large ($\gtrsim 2$) excesses

were previously constrained to less than about 0.5% based on the Trilling et al. (2008) sample. We have set new limits 1-2 orders of magnitude lower and as the left panel of Figure 15 shows, these limits apply to large flux ratios of 10-300.

For the A-type stars (right panel), we show the excess occurrence rate for the single A-star with a W4 excess of 1.63. Of the nine stars in the photospheric flux limited sample without an excess (stars as bright or brighter than the one with an excess), one has an upper limit higher than 1.63, while the others are lower (i.e. the observations could have detected a disk like the one found). The occurrence rate at this flux level therefore lies between 1/9 and 1/10, with these extremes set by assuming that the highest upper limit is either a detection above 1.63 or unity (a non-detection below 1.63). This point is shown as “flux limited” on Figure 15, and is consistent with the sample of Su et al. (2006). With only a single detection this occurrence rate is of course very uncertain.

Considering the full sample of our A-stars yields a lower disk occurrence rate, with at least 145 stars for which this flux ratio could have been detected. If all upper limits are assumed to be non-detections below 1.63 then the occurrence is one from 1672 stars. The vertical line in Figure 15 shows the range set by these two limits, which lies below the point set from the photospheric flux limited sample, and below the distribution of nearby A-stars.

While these two occurrence rates are very uncertain due to only a single disk detection, we consider some possible reasons for the discrepancy. One possibility is an age bias, as most stars in Su et al. (2006) were chosen based on cluster or moving group membership and are therefore younger on average than field A-stars. Cutting the nearby A-star sample to only contain stars older than 400Myr shows that a difference in sample ages has a significant effect on the flux ratio distribution (i.e. disks evolve with time, Rieke et al. 2005; Siegler et al. 2007). Though the extrapolation of the $>400\text{Myr}$ population is very uncertain, this older subsample is more consistent with the WISE excesses from the full sample. The difference in the distributions could therefore be understood if A-stars in the *Kepler* field are typically older than about 400Myr. While there should be no such bias for stars of the same spectral type, there is in fact a difference in the typical spectral types between the *Spitzer* A-star survey and those observed with WISE. While the *Spitzer* sample comprises late B and early A-types, our *Kepler* A-stars are mostly at the lower end of the 7000-10,000K temperature range (i.e. are late A and early F-types). Later spectral types both have lower disk occurrence rates and are typically older due to longer main-sequence lifetimes (e.g. Siegler et al. 2007), which could account for the lower detection rate. It is therefore the higher detection rate inferred from the single WISE excess (around a 9700K star) that may be odd, but given the small number (i.e. 1 disk from 10 stars) can be attributed to chance and that the star with an excess is hotter than most.

5.3 Excess distribution at 12 μm

We have also set stringent limits on the distribution of warm disks at $12\mu\text{m}$. At $12\mu\text{m}$, previous knowledge of the excess distribution was derived from the all-sky IRAS survey (e.g. Aumann & Probst 1991). While many authors have used the results of this survey to discover and study warm excesses (e.g. Song et al. 2005; Chen et al. 2006; Moór et al. 2009; Smith & Wyatt 2010), few have published the results from an unbiased sample at this wavelength in a manner that allows the distribution of the $12\mu\text{m}$ flux ratios to be determined. Figure 16 shows our upper limit on the $12\mu\text{m}$ flux ratio distribution for Sun-like stars, showing that bright ex-

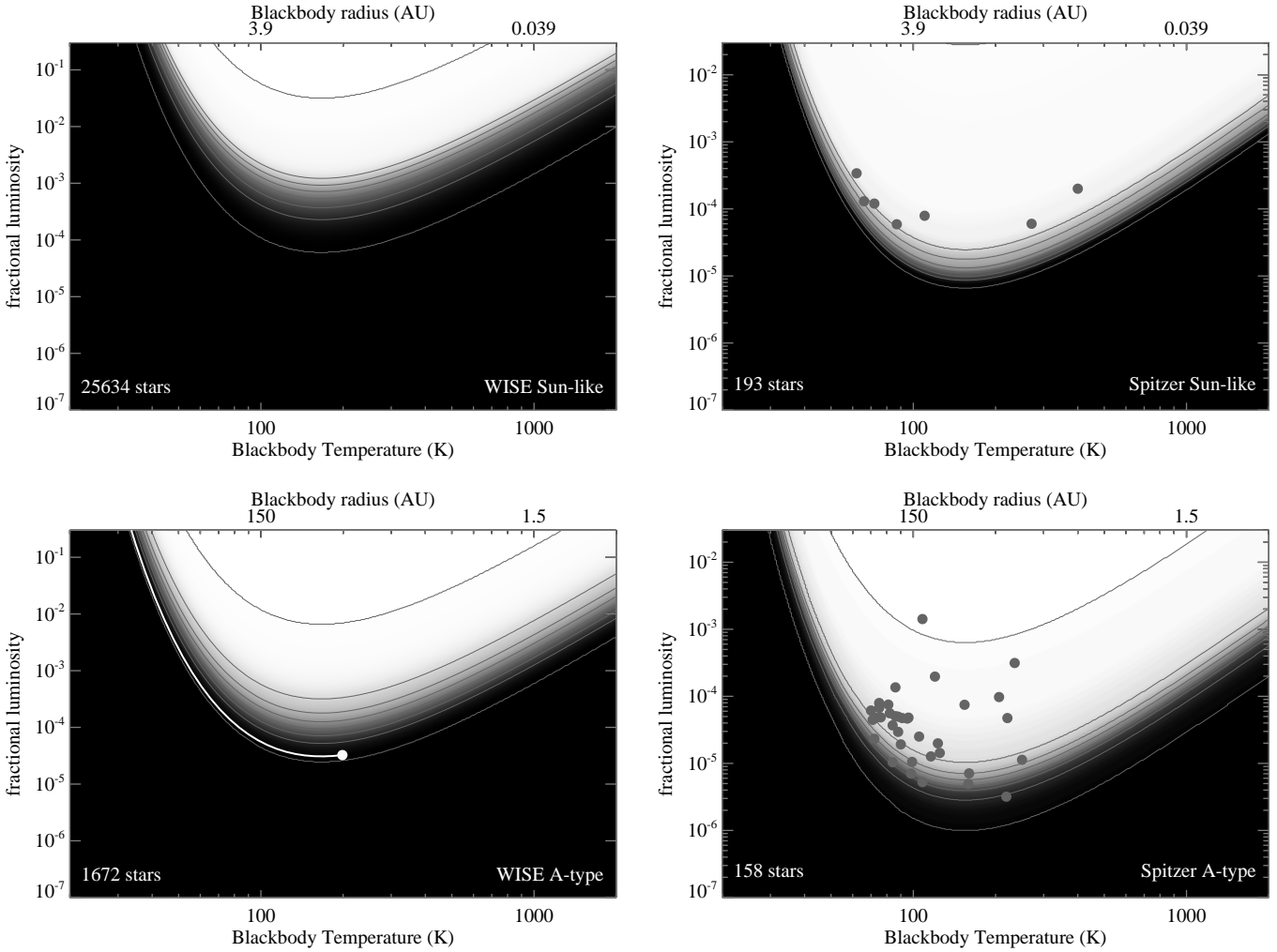


Figure 14. Sun-like (top row) and A-type (bottom row) disk sensitivity comparison between WISE $22\mu\text{m}$ (left column) and nearby stars with *Spitzer* MIPS at $24\mu\text{m}$ (right column). Disks in regions of the parameter space that are white could be detected around all stars, and disks in black regions could not be detected around any star. The colour scale is a linear stretch, contours show 8 linearly spaced levels from 1 to the number of stars observed in each case. The top radial scale assumes $L_\star = 0.5L_\odot$ for Sun-like stars and $L_\star = 20L_\odot$ for A-types. The A-star disk candidate is shown at the temperature fitted in Figure 13, but could lie anywhere along the white line because the temperature is only an approximate upper limit.

cesses at this wavelength are extremely rare. For comparison, we show the lack of excess detection among 71 FGK stars detected at $12\mu\text{m}$ (Aumann & Probst 1991), which was calibration limited and could not detect flux ratios smaller than 1.14. We also show the distribution of IRAS $12\mu\text{m}$ flux ratios for 348 FGK stars in the Unbiased Nearby Star (UNS) sample (Phillips et al. 2010), based on photospheric modelling done for the *Herschel* DEBRIS survey (e.g. Matthews et al. 2010; Kennedy et al. 2012), which has a similar flux ratio sensitivity. The only significant excess is for η Corvi (HD 69830 is the second largest excess, but with a flux ratio of 1.13 is only about 2σ significant).¹¹ These constraints and detections are all consistent, and set limits on the rarity of bright $12\mu\text{m}$ excesses to less than one in every thousand to ten thousand stars for flux ratios greater than about 5.

¹¹ Several other stars in this sample show significant excesses, but these can be shown to be spurious based on more recent *Spitzer* MIPS and *Herschel* PACS observations that resolve the star and a nearby background source.

6 DISCUSSION

One of several goals for this study was to test for a correlation between the existence of debris disks and planets discovered by *Kepler*. However, the distribution of the rare bright excesses that WISE is sensitive to around *Kepler* stars was not known at the outset, so whether this goal was possible was not known either. We noted that even if bright disks were too rare among the bulk population, that a possible correlation between disks and low-mass planets may allow robust disks detections among this subset.

Only one *Kepler* planet candidate host (of 348 KOIs that were not excluded by the $100\mu\text{m}$ background cut) was found to have an excess, so this possibility appears unlikely. In addition, Figure 12 shows that this detection rate is close to that expected from galaxy confusion. Thus, for the bright warm excesses that WISE is sensitive to, there is no evidence that planet host candidates have a disk occurrence rate that is different from the bulk population.

Similarly, excesses around the remaining *Kepler* stars are also consistent with arising from chance alignments with background

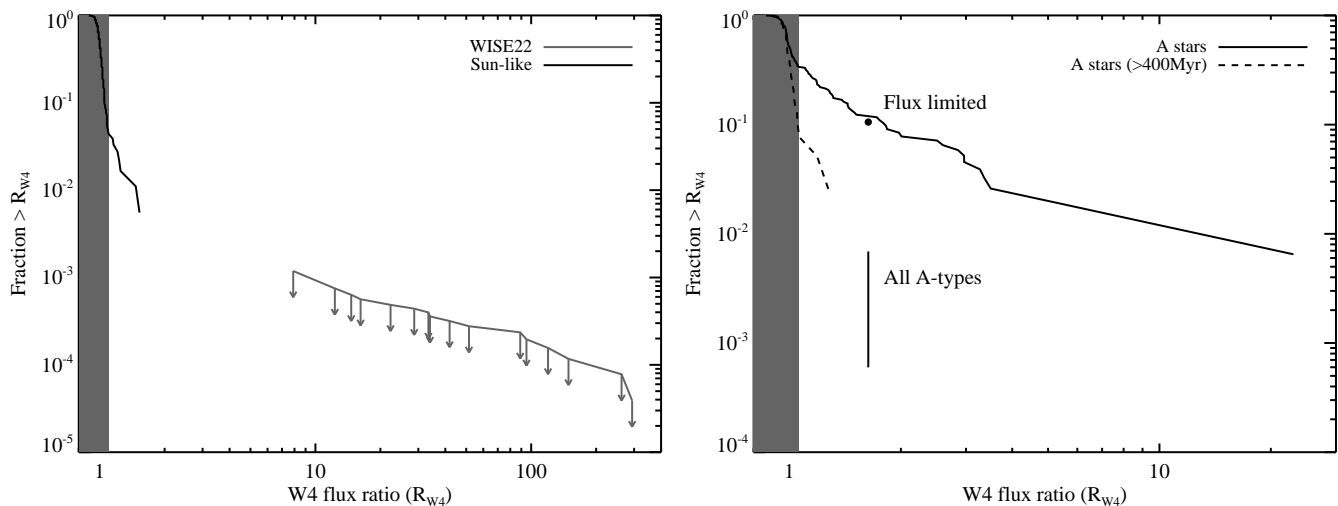


Figure 15. Comparison of 22 and 24 μm flux ratio distributions for WISE and nearby stars (Su et al. 2006; Trilling et al. 2008). The left panel shows Sun-like stars, for which the WISE distribution is an upper limit. The right panel shows A-type stars, and the WISE points are based on the full and flux limited samples and the single disk candidate (see text). We also show a distribution for nearby A-stars older than 400Myr. The dark regions mark where the *Spitzer* observations were calibration limited, below 1.1 (left, Trilling et al. 2008) and below 1.06 (right, Su et al. 2006).

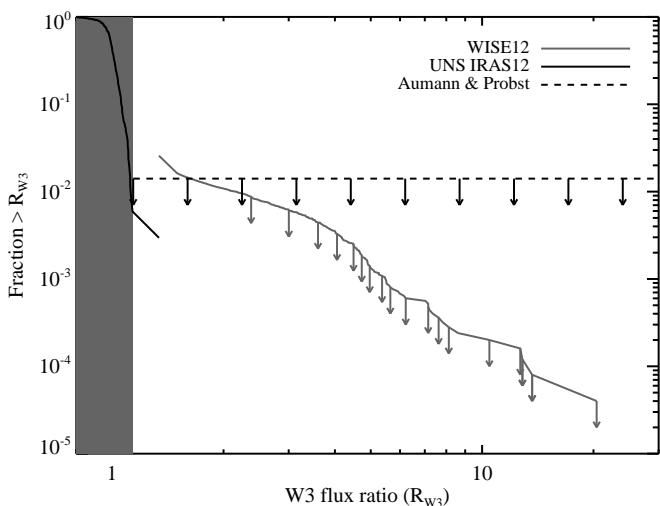


Figure 16. Upper limits on the 12 μm flux ratio distribution from IRAS (dashed line) and WISE (solid grey line), compared to the distribution for stars in the UNS sample using IRAS. The dark region marks where the IRAS detections were calibration limited (below 1.14).

galaxies, with the exception of a single A-type star. However, the possibility that a small number of the excesses are true debris disks means that the chance of detecting transiting dust concentrations is at least as good as for *Kepler* stars without excesses, and may be higher (the 271 *Kepler* stars with W3 or W4 excesses are listed in Table 1). Discovery of many such dust transits that preferentially occur around stars with excesses would argue that at least some excesses are debris disks, though this method of verification seems unlikely.

We have therefore set new limits on the distribution of warm excesses. The range of flux ratios for which we have set limits for Sun-like stars is 2-20 at 12 μm (Fig. 16) and 10-300 at 22 μm (left panel of Fig. 15). For such large 12-22 μm excesses to arise from steady-state processes the planetesimal belts would have to

be either around very young stars or relatively distant from their central star (Wyatt et al. 2007), which in turn requires fractional luminosities $\gtrsim 1\%$ (see Fig. 2). Detecting large warm excesses around main-sequence stars is very unlikely because collisional evolution depletes belts near the central star to undetectable levels rapidly, so the conclusion is that such mid-IR excesses are most likely transient. Two main processes seem to be plausible causes of such excesses. The first, delivery of material from an outer reservoir (Beichman et al. 2005; Wyatt et al. 2007), is appealing because short-lived warm dust can be replenished using material from a long-lived outer belt. Alternatively, because we are here interested in large excesses, the debris from a giant impact between large bodies is a possibility (i.e. perhaps similar to the Earth-Moon forming event, Jackson & Wyatt 2012).

Several possibilities exist for the delivery of objects from an outer belt to terrestrial regions. A system of sufficiently many planets on stable orbits can pass objects inwards from an outer belt (Bonsor & Wyatt 2012), or a planetary system instability can severely disturb a planetesimal population, some of which end up in the terrestrial zone (Gomes et al. 2005). Such possibilities have been suggested as mechanisms to generate the warm dust component observed around η Corvi (Booth et al. 2009; Lisse et al. 2011).

Because at least 15% of Sun-like stars have cool outer planetesimal belts (e.g. Trilling et al. 2008), our limits of 0.01-0.1% for warm belts (for the flux ratios noted above for 12 and 22 μm) mean that fewer than 1 in 150-1500 can be generating large levels of warm dust from cool outer belts at any given time. This fraction could in fact be larger because the 15% only represents disks down to a particular detection limit, and cool disks too faint to detect could still have enough material to produce large warm dust levels (Wyatt et al. 2007). Booth et al. (2009) placed similar limits on the number of systems that could be caught in the act of an instability that delivers large amounts of debris to the terrestrial region, estimating that less than about 0.2% (i.e. 1/500) of Sun-like stars might be observed undergoing an instability at 24 μm .

Whether such instabilities do produce very large excesses is another question. In studying the dust emission generated in their model of the Solar System's proposed planetary instability,

Booth et al. (2009) find that while the relative changes can be very large, the flux ratios are near unity at $12\mu\text{m}$ and of order 10 at $24\mu\text{m}$. However, these ratios may be underestimated because they do not include emission that could arise from the sublimation of comets within 1 AU. It is therefore hard to say whether these results are representative, since they will also depend on the specific system architecture. The η Corvi system has been suggested as a possible candidate currently undergoing such an instability, and shows a $12\mu\text{m}$ flux ratio of 1.3. If typical, these results suggest that instabilities may not produce the larger excesses considered here.

In contrast, the giant impact scenario can produce extremely large excesses (Jackson & Wyatt 2012). The relatively nearby star BD+20 307 (at 96pc), which has a $10\mu\text{m}$ flux ratio of about 100, is a good candidate for such an event (Song et al. 2005; Weinberger et al. 2011). While such events would generally be expected to be associated with young systems, where the final ~ 10 -100 Myr chaotic period of giant impacts and terrestrial planet formation is winding down (e.g. Chambers & Wetherill 1998; Chambers 2001), BD+20 307 is a $\gtrsim 7$ Gyr old main-sequence binary (Zuckerman et al. 2008). The excess may therefore be indicative of a recent instability that has greatly increased the chance of collisions within the terrestrial zone, and is unrelated to planet formation (Zuckerman et al. 2008). Clearly, age estimates for the host stars are important for understanding the origin of dust in such systems.

While the WISE mission might appear to permit near-unlimited sample sizes to help detect the aftermath of the rarest collision events, we have shown that their detection among *Kepler* stars is fundamentally limited. This limit arises because the occurrence rate of excesses that can be detected is too low, so the disks are overwhelmed by galaxy contamination. Because *Kepler* stars represent a sample that will remain unique for the foreseeable future, it is desirable to find ways to overcome this issue. Based on the findings of §4.2, one option is to create sub-samples that maximise the chance of disk detection, because higher disk occurrence rates are more robust to galaxy contamination. Younger stars tend to have larger excesses that are also more frequent (e.g. Rieke et al. 2005; Siegler et al. 2007; Carpenter et al. 2009), so a sub-sample of young stars will be more robust to confusion. The long-term monitoring of *Kepler* stars may provide some help if accurate stellar ages can be derived, for example if rotation periods can be derived to yield age estimates via gyrochronology (Skumanich 1972; Barnes 2007; Mamajek & Hillenbrand 2008). Another way to split the sample is by spectral type, because earlier-type stars are both brighter and have higher disk occurrence rates (for fixed sensitivity). This approach is less appealing for studying the links between disks and planets however, because the bulk of stars observed by *Kepler* are Sun-like.

If we allow for the possibility of observing *Kepler* stars with WISE excesses with other instruments, there is a potential gain with better resolution. A galaxy that is unresolved with WISE might be resolved with *Spitzer*'s IRAC instrument, or using ground-based mid-IR observations on 8m-class telescopes for example. Assuming that it could be detected, the high ($\sim 0''.5$) resolution of such ground-based observations would have over a 99% chance of detecting a galaxy that was not resolved with the WISE beam at $12\mu\text{m}$. Therefore, detection of fewer galaxies than expected in a sample of targets (e.g. significantly fewer than 99 out of 100) would be evidence that the excesses do not randomly lie within the WISE beam and that some are therefore due to excesses centered on the star (i.e. are debris disks).

Ultimately, we found that searching for debris disks around

stars in the *Kepler* field with WISE is limited by the high background level and galaxy contamination. While high background regions can be avoided, background galaxies will always be an issue for such distant stars. Though it means being unable to study the planet-disk connection with such a large planet-host sample, nearby stars should be the focus of studies that aim to better define the distribution of warm excesses. Characterising this distribution is very important, particularly for estimating the possible impact of terrestrial-zone dust on the search for extrasolar Earth analogues (e.g. Beichman et al. 2006a; Roberge et al. 2012). For example, extending the distribution to the faintest possible level available with photometry (calibration limited to a 3σ level of $\sim 5\%$) yields a starting point to make predictions for instruments that aim to detect faint “exozodi” with smaller levels of excess. Because bright warm debris disks must decay to (and be observable at) fainter levels, the distribution will also provide constraints on models that aim to explain the frequency and origin of warm dust.

7 SUMMARY

We have described our search of about 180,000 stars observed by *Kepler* for debris disks using the WISE catalogue. With the completion of the AKARI and WISE missions, such large studies will likely become common. We have identified and addressed some of the issues that will be encountered by future efforts, which mainly relate to keeping spurious excesses to a minimum by using information provided in photometric catalogues.

We used an SED fitting method to identify about 8000 infrared excesses, most of which are in the $12\mu\text{m}$ W3 band around Sun-like stars. The bulk of these excesses arise due to the high mid-IR background level in the *Kepler* field and the way source extraction is done in generating the WISE catalogue. From comparing the number counts for excesses in low background regions with cosmological surveys and WISE photometry from the *Kepler* field, we concluded that a $22\mu\text{m}$ excess around a single A-type star is the most robust to confusion, with about a 1/100 chance of arising due to a background galaxy. We found no evidence that the disk occurrence rate is any different for planet and non-planet host stars.

In looking for these disks we have set new limits on the occurrence rate of warm bright disks. This new characterisation shows why discovery of rare warm debris disks around Sun-like *Kepler* stars in low background regions is generally limited by galaxy confusion. Though the planetary aspect would be lost, nearer stars should be the focus of future studies that aim to characterise the occurrence of warm excesses.

ACKNOWLEDGEMENTS

We thank the reviewer for a thorough reading of this article and valuable comments. This work was supported by the European Union through ERC grant number 279973. This research has made use of the following: The NASA/ IPAC Infrared Science Archive, which is operated by the Jet Propulsion Laboratory, California Institute of Technology, under contract with the National Aeronautics and Space Administration. Data products from the Wide-field Infrared Survey Explorer, which is a joint project of the University of California, Los Angeles, and the Jet Propulsion Laboratory/California Institute of Technology, funded by the National Aeronautics and Space Administration. Data products from the

Two Micron All Sky Survey, which is a joint project of the University of Massachusetts and the Infrared Processing and Analysis Center/California Institute of Technology, funded by the National Aeronautics and Space Administration and the National Science Foundation. The Multimission Archive at the Space Telescope Science Institute (MAST). STScI is operated by the Association of Universities for Research in Astronomy, Inc., under NASA contract NAS5-26555. Support for MAST for non-HST data is provided by the NASA Office of Space Science via grant NNX09AF08G and by other grants and contracts. Data collected by the Kepler mission. Funding for the Kepler mission is provided by the NASA Science Mission directorate.

REFERENCES

- Absil, O. et al. 2006, *A&A*, 452, 237
- Anderson, D. R. et al. 2012, *MNRAS*, 422, 1988
- Aumann, H. H., Beichman, C. A., Gillett, F. C., de Jong, T., Houck, J. R., Low, F. J., Neugebauer, G., Walker, R. G., & Weselius, P. R. 1984, *ApJ*, 278, L23
- Aumann, H. H. & Probst, R. G. 1991, *ApJ*, 368, 264
- Barnes, S. A. 2007, *ApJ*, 669, 1167
- Batalha, N. M. et al. 2010, *ApJ*, 713, L109
- . 2011, *ApJ*, 729, 27
- . 2012, *ArXiv e-prints*, (1202.5852)
- Beichman, C. A., Bryden, G., Gautier, T. N., Stapelfeldt, K. R., Werner, M. W., Misselt, K., Rieke, G., Stansberry, J., & Trilling, D. 2005, *ApJ*, 626, 1061
- Beichman, C. A., Bryden, G., Stapelfeldt, K. R., Gautier, T. N., Grogan, K., Shao, M., Velusamy, T., Lawler, S. M., Blaylock, M., Rieke, G. H., Lunine, J. I., Fischer, D. A., Marcy, G. W., Greaves, J. S., Wyatt, M. C., Holland, W. S., & Dent, W. R. F. 2006a, *ApJ*, 652, 1674
- Beichman, C. A., Tanner, A., Bryden, G., Stapelfeldt, K. R., Werner, M. W., Rieke, G. H., Trilling, D. E., Lawler, S., & Gautier, T. N. 2006b, *ApJ*, 639, 1166
- Beichman, C. A. et al. 2011, *ApJ*, 743, 85
- Bonsor, A. & Wyatt, M. C. 2012, *MNRAS*, 420, 2990
- Booth, M., Wyatt, M. C., Morbidelli, A., Moro-Martín, A., & Levison, H. F. 2009, *MNRAS*, 399, 385
- Borucki, W. J. et al. 2003, in *Society of Photo-Optical Instrumentation Engineers (SPIE) Conference Series*, Vol. 4854, *Society of Photo-Optical Instrumentation Engineers (SPIE) Conference Series*, ed. J. C. Blades & O. H. W. Siegmund, 129–140
- Borucki, W. J. et al. 2011, *ApJ*, 736, 19
- . 2012, *ApJ*, 745, 120
- Brott, I. & Hauschildt, P. H. 2005, in *ESA Special Publication*, Vol. 576, *The Three-Dimensional Universe with Gaia*, ed. C. Turon, K. S. O’Flaherty, & M. A. C. Perryman, 565
- Brown, T. M., Latham, D. W., Everett, M. E., & Esquerdo, G. A. 2011, *AJ*, 142, 112
- Bryden, G., Beichman, C. A., Trilling, D. E., Rieke, G. H., Holmes, E. K., Lawler, S. M., Stapelfeldt, K. R., Werner, M. W., Gautier, T. N., Blaylock, M., Gordon, K. D., Stansberry, J. A., & Su, K. Y. L. 2006, *ApJ*, 636, 1098
- Bryden, G. et al. 2009, *ApJ*, 705, 1226
- Burrows, C. J., Krist, J. E., Stapelfeldt, K. R., & WFPC2 Investigation Definition Team. 1995, in *Bulletin of the American Astronomical Society*, Vol. 27, *American Astronomical Society Meeting Abstracts*, 1329
- Carpenter, J. M. et al. 2009, *ApJS*, 181, 197
- Castelli, F. & Kurucz, R. L. 2003, in *IAU Symposium*, Vol. 210, *Modelling of Stellar Atmospheres*, ed. N. Piskunov, W. W. Weiss, & D. F. Gray, 20P
- Chambers, J. E. 2001, *Icarus*, 152, 205
- Chambers, J. E. & Wetherill, G. W. 1998, *Icarus*, 136, 304
- Chen, C. H., Sargent, B. A., Bohac, C., Kim, K. H., Leibensperger, E., Jura, M., Najita, J., Forrest, W. J., Watson, D. M., Sloan, G. C., & Keller, L. D. 2006, *ApJS*, 166, 351
- Ciardi, D. R., von Braun, K., Bryden, G., van Eyken, J., Howell, S. B., Kane, S. R., Plavchan, P., Ramírez, S. V., & Stauffer, J. R. 2011, *AJ*, 141, 108
- Clements, D. L., Bendo, G., Pearson, C., Khan, S. A., Matsuura, S., & Shirahata, M. 2011, *MNRAS*, 411, 373
- Dodson-Robinson, S. E., Beichman, C. A., Carpenter, J. M., & Bryden, G. 2011, *AJ*, 141, 11
- Doyle, L. R. et al. 2011, *Science*, 333, 1602
- Fujiwara, H., Onaka, T., Ishihara, D., Yamashita, T., Fukagawa, M., Nakagawa, T., Kataza, H., Ootsubo, T., & Murakami, H. 2010, *ApJ*, 714, L152
- Fujiwara, H., Onaka, T., Yamashita, T., Ishihara, D., Kataza, H., Fukagawa, M., Takeda, Y., & Murakami, H. 2012, *ApJ*, 749, L29
- Gaidos, E. J. 1999, *ApJ*, 510, L131
- Gautier, III, T. N. et al. 2007, *ApJ*, 667, 527
- Gomes, R., Levison, H. F., Tsiganis, K., & Morbidelli, A. 2005, *Nature*, 435, 466
- Hines, D. C., Backman, D. E., Bouwman, J., Hillenbrand, L. A., Carpenter, J. M., Meyer, M. R., Kim, J. S., Silverstone, M. D., Rodmann, J., Wolf, S., Mamajek, E. E., Brooke, T. Y., Padgett, D. L., Henning, T., Moro-Martín, A., Stobie, E., Gordon, K. D., Morrison, J. E., Muzerolle, J., & Su, K. Y. L. 2006, *ApJ*, 638, 1070
- Høg, E., Fabricius, C., Makarov, V. V., Urban, S., Corbin, T., Wycoff, G., Bastian, U., Schwekendiek, P., & Wicenc, A. 2000, *A&A*, 355, L27
- Holman, M. J. et al. 2010, *Science*, 330, 51
- Howell, S. B. et al. 2011, *ArXiv e-prints*, (1112.2165)
- Jackson, A. P. & Wyatt, M. C. 2012, *ArXiv e-prints*
- Jarrett, T. H. et al. 2011, *ApJ*, 735, 112
- Kalas, P., Graham, J. R., Chiang, E., Fitzgerald, M. P., Clampin, M., Kite, E. S., Stapelfeldt, K., Marois, C., & Krist, J. 2008, *Science*, 322, 1345
- Kalas, P., Graham, J. R., & Clampin, M. 2005, *Nature*, 435, 1067
- Kennedy, G. M., Wyatt, M. C., Sibthorpe, B., Duchêne, G., Kalas, P., Matthews, B. C., Greaves, J. S., Su, K. Y. L., & Fitzgerald, M. P. 2012, *MNRAS*, 421, 2264
- Kenyon, S. J. & Bromley, B. C. 2005, *AJ*, 130, 269
- Koerner, D. W., Kim, S., Trilling, D. E., Larson, H., Cotera, A., Stapelfeldt, K. R., Wahhaj, Z., Fajardo-Acosta, S., Padgett, D., & Backman, D. 2010, *ApJ*, 710, L26
- Kóspál, Á., Ardila, D. R., Moór, A., & Ábrahám, P. 2009, *ApJ*, 700, L73
- La Franca, F. et al. 2004, *AJ*, 127, 3075
- Lawler, S. M., Beichman, C. A., Bryden, G., Ciardi, D. R., Tanner, A. M., Su, K. Y. L., Stapelfeldt, K. R., Lisse, C. M., & Harker, D. E. 2009, *ApJ*, 705, 89
- Lawler, S. M. & Gladman, B. 2012, *ApJ*, 752, 53
- Lestrade, J.-F., Wyatt, M. C., Bertoldi, F., Dent, W. R. F., & Menten, K. M. 2006, *A&A*, 460, 733
- Lestrade, J.-F., Wyatt, M. C., Bertoldi, F., Menten, K. M., & Labaigt, G. 2009, *A&A*, 506, 1455
- Levison, H. F., Morbidelli, A., Vanlaerhoven, C., Gomes, R., & Tsiganis, K. 2008, *Icarus*, 196, 258

- Lissauer, J. J. et al. 2011a, *Nature*, 470, 53
— 2011b, *ApJS*, 197, 8
- Lisse, C. M., Beichman, C. A., Bryden, G., & Wyatt, M. C. 2007, *ApJ*, 658, 584
- Lisse, C. M., Chen, C. H., Wyatt, M. C., Morlok, A., Song, I., Bryden, G., & Sheehan, P. 2009, *ApJ*, 701, 2019
- Lisse, C. M., Wyatt, M. C., Chen, C. H., Morlok, A., Watson, D. M., Manoj, P., Sheehan, P., Currie, T. M., Thebault, P., & Sitko, M. L. 2011, *ArXiv e-prints*, (1110.4172)
- Louis, C., Mayor, M., Pepe, F., Alibert, Y., Benz, W., Bouchy, F., Correia, A. C. M., Laskar, J., Mordasini, C., Queloz, D., Santos, N. C., Udry, S., Bertaux, J.-L., & Sivan, J.-P. 2006, *Nature*, 441, 305
- Mamajek, E. E. & Hillenbrand, L. A. 2008, *ApJ*, 687, 1264
- Marois, C., Macintosh, B., Barman, T., Zuckerman, B., Song, I., Patience, J., Lafrenière, D., & Doyon, R. 2008, *Science*, 322, 1348
- Matthews, B. C., Sibthorpe, B., Kennedy, G., Phillips, N., Churcher, L., Duchêne, G., Greaves, J. S., Lestrade, J.-F., Moro-Martín, A., Wyatt, M. C., Bastien, P., Biggs, A., Bouvier, J., Butner, H. M., Dent, W. R. F., di Francesco, J., Eislöffel, J., Graham, J., Harvey, P., Hauschildt, P., Holland, W. S., Horner, J., Ibar, E., Ivison, R. J., Johnstone, D., Kalas, P., Kavelaars, J., Rodríguez, D., Udry, S., van der Werf, P., Wilner, D., & Zuckerman, B. 2010, *A&A*, 518, L135
- Miville-Deschênes, M.-A. & Lagache, G. 2005, *ApJS*, 157, 302
- Moór, A., Apai, D., Pascucci, I., Ábrahám, P., Grady, C., Henning, T., Juhász, A., Kiss, C., & Kóspál, Á. 2009, *ApJ*, 700, L25
- Morbidelli, A., Levison, H. F., Tsiganis, K., & Gomes, R. 2005, *Nature*, 435, 462
- Moro-Martín, A., Malhotra, R., Bryden, G., Rieke, G. H., Su, K. Y. L., Beichman, C. A., & Lawler, S. M. 2010, *ApJ*, 717, 1123
- Mouillet, D., Larwood, J. D., Papaloizou, J. C. B., & Lagrange, A. M. 1997, *MNRAS*, 292, 896
- Nesvorný, D., Vokrouhlický, D., & Morbidelli, A. 2007, *AJ*, 133, 1962
- Papovich, C., Dole, H., Egami, E., Le Floch, E., Pérez-González, P. G., Alonso-Herrero, A., Bai, L., Beichman, C. A., Blaylock, M., Engelbracht, C. W., Gordon, K. D., Hines, D. C., Misselt, K. A., Morrison, J. E., Mould, J., Muzerolle, J., Neugebauer, G., Richards, P. L., Rieke, G. H., Rieke, M. J., Rigby, J. R., Su, K. Y. L., & Young, E. T. 2004, *ApJS*, 154, 70
- Phillips, N. M., Greaves, J. S., Dent, W. R. F., Matthews, B. C., Holland, W. S., Wyatt, M. C., & Sibthorpe, B. 2010, *MNRAS*, 403, 1089
- Pilbratt, G. L., Riedinger, J. R., Passvogel, T., Crone, G., Doyle, D., Gageur, U., Heras, A. M., Jewell, C., Metcalfe, L., Ott, S., & Schmidt, M. 2010, *A&A*, 518, L1
- Raymond, S. N., Armitage, P. J., Moro-Martín, A., Booth, M., Wyatt, M. C., Armstrong, J. C., Mandell, A. M., Selsis, F., & West, A. A. 2011, *A&A*, 530, A62
- Ribas, Á., Merín, B., Ardila, D. R., & Bouy, H. 2012, *ArXiv e-prints*, (1203.0013)
- Rieke, G. H. & Lebofsky, M. J. 1985, *ApJ*, 288, 618
- Rieke, G. H., Su, K. Y. L., Stansberry, J. A., Trilling, D., Bryden, G., Muzerolle, J., White, B., Gorlova, N., Young, E. T., Beichman, C. A., Stapelfeldt, K. R., & Hines, D. C. 2005, *ApJ*, 620, 1010
- Roberge, A., Chen, C. H., Millan-Gabet, R., Weinberger, A. J., Hinz, P. M., Stapelfeldt, K. R., Absil, O., Kuchner, M. J., Bryden, G., & the NASA ExoPAG SAG #1 Team. 2012, *ArXiv e-prints*
- Siegler, N., Muzerolle, J., Young, E. T., Rieke, G. H., Mamajek, E. E., Trilling, D. E., Gorlova, N., & Su, K. Y. L. 2007, *ApJ*, 654, 580
- Skrutskie, M. F. et al. 2006, *AJ*, 131, 1163
- Skumanich, A. 1972, *ApJ*, 171, 565
- Smith, B. A. & Terrile, R. J. 1984, *Science*, 226, 1421
- Smith, R. & Wyatt, M. C. 2010, *A&A*, 515, A95
- Smith, R., Wyatt, M. C., & Haniff, C. A. 2009, *A&A*, 503, 265
- Song, I., Zuckerman, B., Weinberger, A. J., & Becklin, E. E. 2005, *Nature*, 436, 363
- Stark, C. C. 2011, *AJ*, 142, 123
- Su, K. Y. L., Rieke, G. H., Stansberry, J. A., Bryden, G., Stapelfeldt, K. R., Trilling, D. E., Muzerolle, J., Beichman, C. A., Moro-Martín, A., Hines, D. C., & Werner, M. W. 2006, *ApJ*, 653, 675
- Su, K. Y. L., Rieke, G. H., Stapelfeldt, K. R., Malhotra, R., Bryden, G., Smith, P. S., Misselt, K. A., Moro-Martín, A., & Williams, J. P. 2009, *ApJ*, 705, 314
- Tenenbaum, P. et al. 2012, *ArXiv e-prints*, (1201.1048)
- Trilling, D. E., Bryden, G., Beichman, C. A., Rieke, G. H., Su, K. Y. L., Stansberry, J. A., Blaylock, M., Stapelfeldt, K. R., Bee-man, J. W., & Haller, E. E. 2008, *ApJ*, 674, 1086
- Verner, G. A., Chaplin, W. J., Basu, S., Brown, T. M., Hekker, S., Huber, D., Karoff, C., Mathur, S., Metcalfe, T. S., Mosser, B., Quirion, P.-O., Appourchaux, T., Bedding, T. R., Bruntt, H., Campante, T. L., Elsworth, Y., García, R. A., Handberg, R., Régulo, C., Roxburgh, I. W., Stello, D., Christensen-Dalsgaard, J., Gilliland, R. L., Kawaler, S. D., Kjeldsen, H., Allen, C., Clarke, B. D., & Girouard, F. R. 2011, *ApJ*, 738, L28
- Weinberger, A. J., Becklin, E. E., Song, I., & Zuckerman, B. 2011, *ApJ*, 726, 72
- Wright, E. L. et al. 2010, *AJ*, 140, 1868
- Wyatt, M. C. 2008, *ARA&A*, 46, 339
- Wyatt, M. C., Smith, R., Greaves, J. S., Beichman, C. A., Bryden, G., & Lisse, C. M. 2007, *ApJ*, 658, 569
- Zuckerman, B., Fekel, F. C., Williamson, M. H., Henry, G. W., & Muno, M. P. 2008, *ApJ*, 688, 1345

APPENDIX A: STARS WITH EXCESSES

Table A1: The 271 *Kepler* stars with WISE 3-4 excesses. Columns are: KIC identifier, predicted *Kepler* (K_p) magnitude from the KIC, Quarters the star was observed in, fitted effective temperature, W3-4 flux ratio and excess significance (where $X_{W3,4} \geq 4$). The note column notes the single KOI, and potential planet hosts from [Tenenbaum et al. \(2012\)](#) (“T12”).

KIC	K_p	Quarters	T_{eff}	R_{W3}	X_{W3}	R_{W4}	X_{W4}	Notes
5866211	15.19	456	6585	4.2	5.0			
5866341	15.06	123456	6296	4.9	6.7			
5866415	15.33	123	6029	4.7	4.4			
6198278	14.86	123456	5436	2.8	4.1			
6346886	14.96	12346	5869	3.9	4.6			
6431431	14.87	123456	8147	5.9	7.8			
6503763	15.78	12346	5275	4.3	4.1			
6515382	13.29	123456	6265	1.7	4.2			
6516101	13.88	123456	6062	2.3	6.1			
6599949	15.42	123456	5773	4.0	4.1			
6676683	14.58	123456	6356	4.1	6.2			
6685526	15.00	123456	5103	2.7	4.1			KOI 861,T12
6773853	14.89	123456	6041	2.9	4.0			
6935614	15.73	123456	5832	7.1	7.1			
7022341	15.52	456	6111	5.1	4.4			
7104629	15.41	123456	5824	4.9	4.6			
7104793	15.51	123456	5013	3.6	4.8			
7184587	15.61	123456	3963			33.2	4.1	
7187014	15.46	123456	5940	4.9	5.1			
7187096	15.07	123456	4153	2.0	4.9			
7189185	15.18	123456	5359	4.9	5.9			
7268366	14.52	123456	6034	4.6	7.7			
7345479	7.93	123456	9686			1.6	4.5	
7349062	14.90	123456	6606	3.8	4.7			
7349090	14.76	123456	6173	4.1	6.2			
7350204	14.85	1256	6385	3.7	4.6			
7354462	15.29	123456	6388	4.5	4.5			
7516798	15.10	123456	5582	3.1	4.0			
7581686	12.61	123456	6342	1.9	7.4	14.7	5.8	
7593434	14.92	123456	5559	3.3	5.1			
7595932	13.44	123456	5039	2.5	9.8			
7597096	15.78	256	6273	6.2	4.7			
7659091	13.57	123456	5844	1.8	4.5			
7667940	14.48	123456	5716	3.3	6.2			
7673565	15.62	23	6363	5.5	4.7			
7730130	16.17	2	4860	4.9	4.6			T12
7731810	15.55	2	7482	3.8	4.2			
7744202	15.52	456	5246	4.0	4.6			
7744209	15.70	123456	5143	5.0	5.1			
7746956	15.27	123456	6976	4.7	5.0			
7808214	15.49	123456	4611	4.3	9.6			
7811074	15.43	123456	5742	4.5	4.5			
7877878	15.86	456	6026	7.2	4.7			
7877962	14.46	123456	5937	2.4	4.1			
7879639	15.90	123456	4896	5.5	5.7			
8005470	14.18	123456	5608	2.0	4.3			
8013236	15.72	23456	5241	4.6	4.6			
8016698	13.45	123456	7910	2.0	4.9			
8075618	15.67	123456	5666	4.5	4.3			T12
8077083	15.92	123456	5456	12.7	10.2	293.7	9.2	
8085263	15.76	23456	6369	12.9	8.5			
8145154	14.09	123456	6144	2.2	4.8			
8145181	14.98	123456	5240	2.6	4.5			

KIC	K_p	Quarters	T_{eff}	R_{W3}	X_{W3}	R_{W4}	X_{W4}	Notes
8153997	15.14	123456	5841	3.5	4.8			
8212592	16.66	2	3840	3.6	5.5			
8213938	13.14	123456	5650	1.8	5.8			
8284699	15.42	123456	5303	3.8	4.1			
8284814	14.92	123456	6368	3.2	4.3			
8345414	15.29	123456	4184	2.0	4.0			
8349926	14.78	123456	5819	2.6	4.2			
8350421	15.69	123456	4674	2.7	4.3			
8351168	13.93	123456	5230	2.3	7.5			
8410210	15.36	123456	5957	4.7	4.1			
8410749	15.01	456	6608	4.9	7.3			
8417035	15.84	456	4680	3.4	4.0			
8607558	15.29	123456	5937	3.7	4.4			
8611027	15.56	23456	4869	3.5	5.0			
8612202	14.56	123456	8504	2.6	4.4			
8612850	15.29	123456	6206	5.3	6.2			
8672241	14.03	123456	5852	2.2	5.0			
8736331	15.86	123456	6269	7.4	5.9			
8736639	14.73	123456	5092	2.2	4.2			
8741807	15.15	123456	6855	4.2	4.6			
8800998	13.72	123456	9000	6.7	10.3			
8803050	13.92	123456	6376			34.0	4.4	
8807242	14.31	123456	5850	2.7	4.5			
8870902	13.55	123456	6342	2.4	5.5			
9071384	15.64	123456	4734	3.3	4.9			
9074768	14.72	123456	5915	8.1	12.9	89.0	6.1	
9074812	14.53	123456	5961	2.3	4.2			
9076617	14.49	123456	5921	2.5	4.3			
9137443	13.76	123456	5879	1.9	4.6			
9138286	14.15	123456	5603	2.1	4.3			
9139782	15.76	456	5949	5.0	5.0			
9142411	15.19	123456	5953	4.2	4.0			
9206761	15.82	23456	6021	7.2	5.0			
9264468	14.36	123456	5440	2.1	4.3			
9267353	14.78	123456	6200	3.8	6.4			
9269492	14.64	123456	4856	2.4	5.8			
9328535	13.87	123456	5900	1.8	4.6			
9329967	13.35	123456	6356	2.8	9.3			
9452213	13.40	123456	8410	1.7	4.8			
9511303	14.95	123456	5975	2.9	4.3			
9511944	14.12	123456	6364	2.3	4.3			
9512868	13.86	23456	5289	2.3	6.5			
9575361	15.86	123456	4139	4.1	7.8			
9691491	15.75	123456	4117	2.3	4.0			
9703058	16.77	5	3995	4.4	5.2			
9762054	15.84	456	6044	5.6	4.2			
9813767	15.99	123456	5039	4.8	4.9			
9823991	15.74	123456	5520	5.4	5.0			
9824039	14.99	123456	5487	3.5	4.1			
9873729	13.55	123456	3903	1.3	4.4			
9873862	15.28	123	5040	2.8	4.5			
9875170	15.28	123456	5469	2.9	4.3			
9875827	15.36	123456	5114	5.7	8.7			
9883553	12.93	123456	6586	1.6	4.5			
9883654	14.96	123456	6351	3.2	4.3			
9883689	14.74	123456	5409	2.7	5.4	33.4	4.0	
9883939	14.82	123456	5852	3.0	4.4			
9933368	15.03	123456	6037	5.5	7.0			
9933625	12.82	123456	5550	1.5	5.0			
9936573	14.62	123456	5527	2.4	4.5			
10002543	13.24	123456	7313	1.7	4.5			

KIC	K_p	Quarters	T_{eff}	R_{W3}	X_{W3}	R_{W4}	X_{W4}	Notes
10002794	15.96	23456	5259	7.0	5.1			
10056410	15.24	123456	5778	3.5	4.3			
10062742	15.77	23	6370	5.6	5.5			
10063763	13.31	123456	7532	2.0	6.1			
10065701	14.51	123456	6145	2.6	4.7			
10119646	15.74	123456	5418	4.7	4.9			
10120908	15.83	123456	4915	4.3	5.3			
10128226	15.16	123456	6157	4.5	5.4			
10128466	13.18	1	6249	1.7	4.2			
10128553	15.18	123456	5428	4.1	5.2			
10128580	15.44	123456	5208	3.7	4.3			
10128587	15.17	123456	4813	2.5	4.7			
10131814	14.15	123456	5415	2.1	4.9			
10192175	15.12	123456	5624	3.9	5.3			
10195974	14.96	123456	5539	3.0	4.4			
10199239	13.66	123456	5605	1.9	4.4			
10199401	15.49	123	5556	6.1	7.7			
10252275	13.75	123456	5132	1.5	4.1			
10252286	14.94	123456	6057	4.0	6.1			
10252364	13.55	123456	5984	1.7	4.2			
10253878	15.86	456	6377	7.8	6.7			
10255817	15.37	123456	5071	4.7	6.7			
10256442	15.48	123456	5469	3.7	4.4			
10256507	14.91	123456	5119	2.5	4.7			
10264259	14.92	123456	4967	2.6	6.0			
10265238	15.08	123456	5767	2.8	4.7			
10265241	15.11	123456	5631	3.1	4.9			
10265602	15.55	23456	5855	4.8	5.0			
10318128	14.80	123456	6628	4.0	5.8			
10321367	15.22	123456	6176	4.7	5.4			
10321406	14.95	123456	5853	3.3	5.2			
10321407	15.30	456	6306	3.9	4.2			
10321422	15.06	123456	4832	2.5	4.8			
10322187	15.69	23	5578	4.7	4.1			
10322220	15.30	456	5028	2.8	4.7			
10328472	14.72	123456	5934	2.7	4.1			
10330579	14.53	123456	6281	2.4	4.4			
10382415	15.63	56	4073	3.6	8.9			
10383222	15.51	23456	4959	2.9	4.1			
10386716	16.86	2	4844	10.5	6.1			
10386900	14.88	123456	5583	2.7	4.3			
10387564	15.35	123456	5909	4.0	4.6			
10395762	15.50	123456	6072	4.1	4.0			
10395814	15.89	456	4806			95.1	4.4	
10447798	14.74	123456	5241	2.4	5.0			
10451070	15.00	123456	5038	2.4	4.0			
10451135	14.24	123456	5354	2.3	5.2			
10451251	15.66	456	4705	3.1	5.2			
10451497	15.20	123456	5460	3.2	4.7			
10451632	15.33	123456	4771	2.8	5.3			
10461970	15.77	123456	5645	5.5	4.8			
10513479	14.97	123456	8410	6.4	9.8			
10513812	14.41	123456	6256	2.5	4.8			
10515235	15.53	23456	5924	5.0	5.1			
10515276	15.26	123456	3917	2.2	7.4			
10516147	14.84	123456	6136	3.6	6.5			
10516255	15.34	123456	5948	4.1	5.2			
10517028	13.48	123456	6630	2.0	4.8			
10517486	15.35	1256	5050	2.9	4.4			
10579318	15.42	123456	5304	3.5	4.3			
10580355	14.78	123456	5473	3.2	5.9			

KIC	K_p	Quarters	T_{eff}	R_{W3}	X_{W3}	R_{W4}	X_{W4}	Notes
10580447	15.84	123456	3987	2.7	5.8			
10580525	13.86	123456	6388	2.0	4.6			
10580779	15.64	123456	5470	4.5	5.7			
10580786	15.38	123	5897	5.0	5.9			
10581163	13.60	123456	5973	1.7	4.4			
10581308	13.77	123456	5460	1.8	5.1			
10581836	15.39	123456	4841	3.8	6.8			
10582786	14.68	123456	5765	2.3	4.3			
10583400	14.86	123456	5217	2.4	4.6			
10583563	14.11	123456	5482	1.8	4.3			
10591195	14.67	123456	5941	3.6	6.5			
10644697	14.17	123456	6396	2.3	5.3			
10645900	15.83	145	5624	4.2	4.0			
10645926	14.33	123456	6393	2.2	4.1			
10646068	17.51	6	3813	5.5	4.3			
10646091	15.04	123456	4117	1.8	4.8			
10646106	15.33	123456	5585	3.4	4.6			
10646263	15.56	123456	6091	5.9	5.5			
10646283	15.40	123456	5465	3.9	4.7			
10646426	14.69	123456	4768	1.8	4.3			
10646589	14.62	123456	5149	2.5	5.4			
10649444	15.37	456	3900	1.6	4.1			
10649541	15.63	123456	5704	4.2	4.9			
10649562	14.14	123456	5436	2.1	5.5			
10656438	15.99	123456	4574	3.0	4.7			
10710753	15.50	123456	4044	1.9	4.3			
10711021	15.96	123456	4852	4.1	5.0			
10711045	15.88	123456	4857	3.4	4.3			
10711052	15.53	123456	4924	4.5	7.1			
10711088	14.03	6	6153	2.4	5.0			
10711259	15.16	123456	6207	3.4	4.0			
10711510	15.02	123456	6210	3.2	4.1			
10714422	15.33	123456	4759	2.4	4.6			
10714459	15.58	23	6000	6.0	6.4			
10714581	13.95	145	4388	1.5	5.5			
10716598	14.37	123456	5350	2.0	4.0			
10721855	13.86	123456	5212			16.2	4.0	
10722535	15.84	123456	5348	5.5	5.1			
10724544	15.01	123456	5546	5.1	8.0			
10777410	15.09	123456	3900	1.4	4.4			
10777448	15.71	123456	4067	2.4	5.4			
10777591	13.33	123456	5517	2.2	8.1			
10777728	15.15	123456	6080	3.6	4.5			
10778016	15.24	123456	5919	3.8	4.5			
10845333	15.64	123456	5221	3.7	4.8			
10907059	14.50	123456	6276	2.5	4.1			
10907132	15.68	23456	6167	4.6	4.3			
10908054	13.44	123456	6353	2.0	5.4			
10958951	12.67	123456	6459	2.4	9.9	12.3	4.4	
11017907	11.80	123456	5873			7.9	6.7	
11074521	15.57	123456	4921	3.7	5.7			
11075222	14.33	123456	5593	2.4	5.8			
11086203	14.30	123456	6543	2.9	6.1			
11086359	15.83	456	6052	4.7	4.1			
11125136	15.33	123456	5767	4.5	5.5			
11180691	15.94	456	5065	4.0	4.1			
11181653	15.25	123456	5936	3.8	4.6			
11190125	13.75	123456	6737	1.9	4.4			
11288574	13.46	123456	5408	1.7	5.6			
11296807	15.06	123456	6036	4.3	6.3			
11341446	13.42	123456	5553	1.6	4.5			

KIC	K_p	Quarters	T_{eff}	R_{W3}	X_{W3}	R_{W4}	X_{W4}	Notes
11393569	15.99	123456	4563	3.3	4.8			
11401060	15.36	123456	7981	12.3	13.0			
11401954	13.21	123456	5870	1.6	4.3			
11404100	15.00	123456	5045	2.3	4.5	41.9	5.2	
11442840	15.07	123456	5322	3.5	5.6			
11444855	15.10	145	5642	4.2	6.3			
11456355	13.57	123456	7298	1.8	4.4			
11457002	15.94	2	5889	4.7	5.6			T12
11457020	14.90	123456	6120	2.7	4.4			
11457038	14.32	123456	5744	2.2	5.1			
11493473	13.63	123456	6125	3.2	10.3	22.3	4.8	
11493497	15.41	123456	3897	2.3	8.5			
11507003	12.67	123456	5467	1.3	4.2			
11507053	15.84	456	5565	5.3	5.7			
11507127	14.27	123456	5925	3.0	7.3	28.7	4.1	
11507139	15.94	2456	5979	8.6	7.2			
11546374	15.74	123456	3854	1.9	4.9			
11546397	15.99	123456	4758	3.3	4.3			
11551210	12.83	123456	5863	3.3	9.0			
11558249	15.17	123456	6210	3.6	4.5			
11598638	13.73	123456	6165	3.5	9.1			
11649347	15.93	123456	5043	7.6	8.3	148.9	5.9	
11649744	13.88	123456	5014	2.1	7.4			
11700640	15.24	123456	6151	4.2	4.6			
11753371	15.42	123456	5527	4.4	6.5			
11803544	15.14	123456	5038	2.7	4.8			
11855348	15.21	456	6286	13.7	15.2	119.7	5.9	
11855417	13.80	123456	5841	1.8	4.2			
11903173	14.99	12356	4938	3.0	6.3			
12053791	15.46	123456	5721	3.9	4.4			
12056198	15.68	123456	5577	20.4	15.6	262.3	9.1	
12058865	14.42	123456	6125	3.1	6.1	51.5	4.9	
12058904	14.88	145	5095	3.4	7.1			
12350553	14.53	123456	5935	3.5	7.1			
12506956	15.09	123456	5030	2.7	4.9			